HHS Public Access

Author manuscript

Cell Rep. Author manuscript; available in PMC 2024 August 02.

Published in final edited form as:

Cell Rep. 2022 December 20; 41(12): 111838. doi:10.1016/j.celrep.2022.111838.

A molecular atlas of the human postmenopausal fallopian tube and ovary from single-cell RNA and ATAC sequencing

Ernst Lengyel[1,5,6,*], **Yan Li**[2,5], **Melanie Weigert**[1], **Lisha Zhu**[2], **Heather Eckart**[3], **Melissa Javellana**[1], **Sarah Ackroyd**[1], **Jason Xiao**[1], **Susan Olalekan**[3], **Dianne Glass**[1], **Shilpa Iyer**[1], **Rahul Krishnan**[1], **Agnes Julia Bilecz**[4], **Ricardo Lastra**[4], **Mengjie Chen**[3,5,*], **Anindita Basu**[3,5,*]

[1]Section of Gynecologic Oncology, Department of Obstetrics and Gynecology, The University of Chicago, Chicago, IL 60637, USA

[2]Center for Research Informatics, The University of Chicago, Chicago, IL 60637, USA

[3]Section of Genetic Medicine, Department of Medicine, The University of Chicago, Chicago, IL 60637, USA

[4]Department of Pathology, The University of Chicago, Chicago, IL 60637, USA

[5]These authors contributed equally

[6]Lead contact

SUMMARY

As part of the Human Cell Atlas Initiative, our goal is to generate single-cell transcriptomics (single-cell RNA sequencing [scRNA-seq], 86,708 cells) and regulatory (single-cell assay on transposase accessible chromatin sequencing [scATAC-seq], 59,830 cells) profiles of the normal postmenopausal ovary and fallopian tube (FT). The FT contains 11 major cell types, and the ovary contains 6. The dominating cell type in the FT and ovary is the stromal cell, which expresses aging-associated genes. FT epithelial cells express multiple ovarian cancer risk-associated genes (*CCDC170*, *RND3*, *TACC2*, *STK33*, and *ADGB*) and show active communication between fimbrial epithelial cells and ovarian stromal cells. Integrated single-cell transcriptomics and chromatin accessibility data show that the regulatory landscape of the fimbriae is different from other anatomic regions. Cell types with similar gene expression in the FT display transcriptional

*Correspondence: elengyel@uchicago.edu (E.L.), mengjiechen@uchicago.edu (M.C.), onibasu@uchicago.edu (A.B.).

AUTHOR CONTRIBUTIONS

E.L., A.B., and M.C. jointly oversaw project design and analysis. Y.L., L.Z., and M.C. performed all computational analyses. H.E., M.J., S.A., J.X., R.K., M.W., and S.O. performed experiments, including tissue dissociation, Drop-seq, and 10x Genomics scRNA and ATAC-seq assays. M.W. performed the FISH experiments. R.L. and A.J.B. read histology and immunohistochemistry. D.G. and S.I. obtained consent and performed the surgeries on all women donating the tissue. E.L., A.B., M.W., and M.C. wrote the manuscript. All authors reviewed and agreed on the final version of the submitted manuscript.

SUPPLEMENTAL INFORMATION

Supplemental information can be found online at https://doi.org/10.1016/j.celrep.2022.111838.

DECLARATION OF INTERESTS

E.L. receives research funding to study ovarian cancer from Arsenal Bioscience and AbbVie through the University of Chicago unrelated to this work. A.B. is a consultant for Novartis IBRI.

profiles. These findings allow us to disentangle the cellular makeup of the postmenopausal FT and ovary, advancing our knowledge of gynecologic diseases in menopause.

In brief

Lengyel et al. present a single-cell atlas of the normal postmenopausal ovary and fallopian tube and identify crosstalk between the two organs as well as expression of putative disease genes.

Graphical Abstract

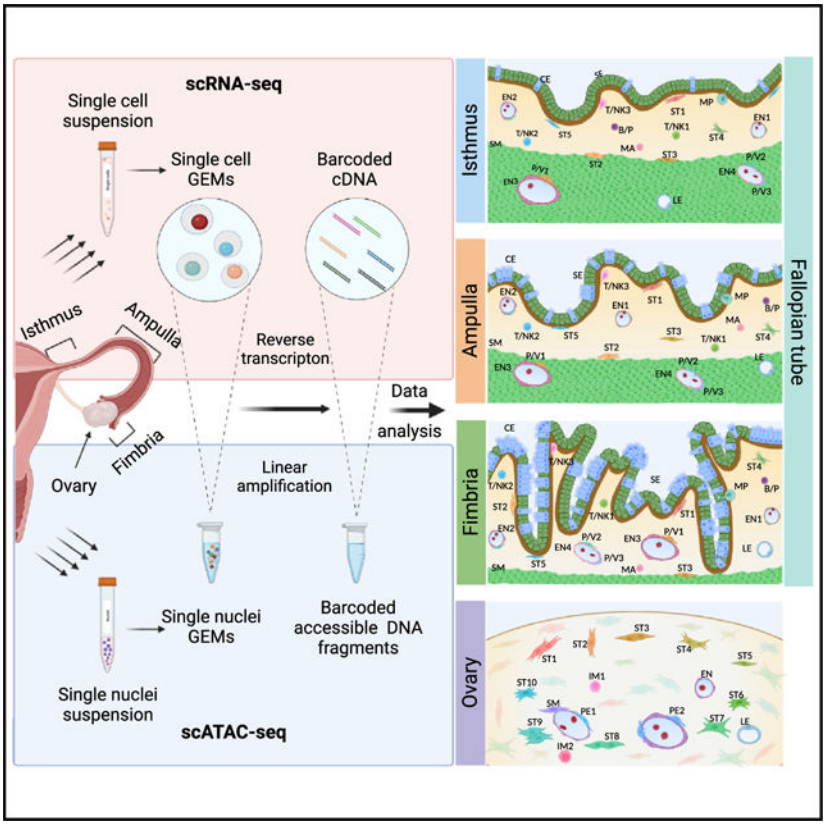

INTRODUCTION

The first step toward a better understanding of the etiology of tubal and ovarian diseases, which often surface after menopause, is to create a comprehensive map of the normal anatomy and cellular composition of these organs. The three main areas of the fallopian tube explored in this study are (1) the isthmus, a short section with a thick muscular wall that is closest to the uterus and merges with (2) the ampulla, a longer, thinner-walled central portion, which connects to (3) the fimbriated end, shaped like the bell of a trumpet and fringed with fimbria, which opens and is in close contact with the ovary (Figure 1A). The entire tube is composed of three layers. The innermost is an epithelial/mucosal layer lining a central muscular layer, consisting mostly of smooth muscle cells, which lines the third layer, an outer surface covered by serosa. There are no major histological differences between the pre- and postmenopausal fallopian tube. In contrast, the postmenopausal ovary differs

dramatically from the premenopausal ovary in that it is mostly fibrotic with atretic follicles, covered by a single layer of cuboidal epithelial cells, which detaches easily during surgical manipulation. During the reproductive years, the biological functions of the ovary include hormone production, oocyte maturation, and immune defense,[1,2] but its postmenopausal functions and cellular compositions are less well defined.

Some diseases seen in premenopausal women, like endometriosis and the early steps of epithelial ovarian cancer, persist or become clinically manifest in menopause. Ovarian cancer is a deadly disease threatening the health of postmenopausal women.[3] There are more than 30 histological subtypes of benign, borderline, and malignant ovarian tumors listed in the World Health Organization (WHO) clinical staging system, and many of these have no identified cell of origin. The most common subtype, epithelial high-grade serous ovarian cancer, is now believed to arise from the epithelial cells in the fallopian tube; however, there is still uncertainty because stromal cells may also play a role in the origin of the disease.[4,5] A comprehensive characterization of all cell types in the normal postmenopausal fallopian tube and ovary might contribute to understanding how these organs undergo malignant transformation.

Single-cell techniques have quickly expanded our understanding of the underlying cellular heterogeneity of ovarian cancer, but there is limited information about the cellular composition of the fallopian tube and ovary. Most current studies have been limited to single-cell RNA sequencing (scRNA-seq). Although these reports provide critical information, it is becoming increasingly evident that gene expression data alone may not adequately define cell types or elucidate the transcriptional regulations involved in development, maintenance, and aging of the female reproductive system. Epigenetic information, such as chromatin accessibility, is likely essential for depicting a more complete regulatory landscape. In this study, we used a combination of single-cell gene expression and chromatin accessibility assays, including Drop-seq, 10x scRNA-seq, and single-cell assay on transposase accessible chromatin sequencing (scATAC-seq), to generate a high-quality cell atlas that consists of four tissue sites from the reproductive tract of postmenopausal women. This atlas, by far the most comprehensive map of the postmenopausal female reproductive system to date, will pave the way for a better understanding of the pathophysiology of many diseases affecting older women.

RESULTS

Characterizing canonical cell types in the postmenopausal fallopian tube and ovary

This study of the normal postmenopausal fallopian tube and ovary included 8 non-smoking postmenopausal women over 55 years of age undergoing surgery to treat vaginal prolapse without any major macroscopic and histologic abnormality (Table S1). Fresh tissues were transported expeditiously from the operating room to the laboratory for cell dissociation and used for scRNA-seq and scATAC-seq. To ascertain changes in cell type, gene expression, and chromatin accessibility over the length of the fallopian tube (approximately 11 cm), tissue samples were taken from the isthmus, which is close to the uterus; the ampulla, which is mid-tube; and the fimbriae, at the end of the tube (Figure 1A).

In total, 18 fallopian tube tissue samples from 7 donors were profiled using scRNA-seq. Among them, 5 tissue samples from 2 donors (donor 1 [D1] and D2) were processed using Drop-seq, and the remaining were processed using 10X Genomics. After removing doublets and cells with high mitochondrial content, 60,574 cells from all three anatomic sites of the fallopian tube (FT) were retained for cross-sample integration and downstream analysis. We identified 22 clusters (Figure 1B) across the three anatomic subsections of the FT and all donors, using unsupervised clustering and canonical marker genes (Figure S1A; Table S2). The 22 FT clusters were classified into 11 major cell types (Figure S1B) based on expression of marker genes (Table S3): ciliated epithelial (CE), secretory epithelial (SE), smooth muscle (SM), pericyte/vascular (P/V1–P/V3), endothelial (EN1–EN4), lymphatic EN (LE), stromal (ST1–ST5), mast (MA), and 3 immune cell types: T and natural killer (NK) cells (T/NK1–T/NK3), macrophages (MP), and B and plasma (B/P) cells. Significant differences in gene expression were seen between the different subgroups of P/V cells (Figure S1A). SE and CE cells could not be further subclustered using scRNA-seq, which was not the case in studies of FT tissue from premenopausal patients[6,7] (Figure S1A). Although all ST cells expressed *COL1A1* and *PDGFRA*, 2 subgroups become apparent. ST1/3/4 strongly expressed the mediators of Wnt signaling POSTN and SFRP4. ST2/5 expressed *DCN*, *NCAM1*, *CD99*, and a stem cell marker, *CD34* (Figures 1C, S1A, and S1C).

The uniform manifold approximation and projection (UMAP) clustering analysis (Figure 1B) worked well in the definition of major cell types but failed to resolve finer subclusters within some major cell types, such as T and NK cells. We therefore applied an alternative approach, heterogeneity-induced-pre-processing tool (HIPPO), which can resolve cellular heterogeneity by iterative feature selection and clustering.[8] HIPPO applies a hierarchical strategy and represents each new cluster using a different set of markers (Table S3) by a zero-inflation test. When HIPPO was applied to T and NK cells for finer subclustering, multiple subsets of T cells were revealed, including CD4+ T cells, CD4+ regulatory T cells, and CD8+ T cells (Figure 1C). Two subclusters from this analysis can be attributed to CD8+ T cells by expression of *CD8A* and *CD8B*. *PDCD1*, *TOX*, and *LAG3* were expressed in one CD8+ T cell cluster but were not expressed or weakly expressed in the other, suggesting that this second cluster might represent a subpopulation of exhausted CD8+ cells.[9] We also noted expression of *CD99* or *MIC2,* immune-related genes that increase T cell adhesion and apoptosis, in ST2 and ST5 cells, and *CD24,* a cancer stem cell marker, in SE and CE cells.

scRNA-seq was also performed on the ovaries of 6 donors using Drop-seq (D1 and D2) and the 10X genomics (D3, D5, D7, and D8) assay. We did not find evidence of epithelial cells because the ovary is covered by a single layer of ovarian surface epithelial cells (Figure 1D) that comes off during surgery. After removing doublets and high-mitochondrial-content cells, we obtained 26,134 ovarian cells for downstream analysis. Unsupervised clustering of the cells from the ovaries across donors yielded 17 clusters (Figures 1E and S1D; Tables S3 and S4), which were classified into 6 major cell types (Figure S1E; Table S3) using selected marker genes: ST1–ST10), perivascular EN (PE1 and PE2), SM, EN, LE, and immune (IM1 and IM2) cells. Consistent with the high expression of the known ST marker decorin (*DCN*) in ST cells in scRNA-seq, most ST cells in the ovary expressed DCN, as shown using RNA

fluorescence *in situ* hybridization (FISH) (Figure S1F). Most cells in the ovary are ST cells, but there is an unexpectedly large fraction of PE cells (Figures 1D and 1E).

For the FT and ovary, there was some variability in cell type composition between donors (Figures 1F and 1G; Table S5), but in general, they followed the overall cell type composition seen in the computationally pooled samples. The ovary and FT expressed no oocyte markers (Figure S1G), consistent with the postmenopausal state of the ovaries.[10] There was no appreciable difference in cell types or composition between Drop-seq and 10x Genomics 3′ RNA-seq data for both organs.

We compared our FT scRNA-seq dataset with 2 published datasets of scRNA-seq[7,11] in the FT (Figure S1H). There was minimal overlap in UMAP space with fresh and cultured FT epithelial cells from Hu et al.,[11] possibly because of different single-cell sequencing approaches. However, we found significant overlap with the scRNA-seq profile from one postmenopausal donor in the Dinh et al.[7] study. Comparing our data with the published studies, we see significant overlap in expression of genes implicated in high-grade serous ovarian cancer (data not shown).

Characterization of the different anatomic regions in the postmenopausal FT

Driven by known structural and functional differences in anatomic regions, we characterized the three anatomic regions, the isthmus, ampulla, and fimbriae of the FT (Figures 1A and 2A), at the cellular and molecular levels (Figures 2B and 2C). Overall, each major cell type was present in roughly similar proportions in all three regions of the FT (Figures 2A and 2B). Figure 2C shows the normalized expression levels of key genes in the major cell types of the isthmus/ampulla/fimbriae and the percentage of cells in the respective clusters expressing them. SE and CE cells shared several pan-epithelial cell markers (*EPCAM*, *KRT8/18/19*, *FOLR1*, *SLPI*, *WFDC2,* and *E-cadherin* [*CDH1*]) in all anatomic regions.[12] SE cell-specific markers present in all three anatomic regions that were not expressed in ciliated cells included *KRT7*, *OVGP1*, and *MSLN*. The complement gene *C3* and the tumor suppressor gene *CSMD1* were reduced in SE cells of the fimbriae (Figure 2C). Expression of markers specific to CE cells included known markers[7] (*CAPS* and *FOXJ1*) and new markers (*PIFO*, *TMEM190*, and *SNTN*). The histone-related gene *HIST1H4C* is expressed in CE cells of the isthmus but not in the ampulla and the fimbria. Reticulon 1 (*RTN*-1), important for cell apoptosis and part of a SNP increasing colorectal cancer risk,[13] was not expressed in CE cells of the fimbriae (Figures 2C and S2B).

Although the three regions (Figures 1A and 2B) essentially share a similar pattern of major cell types, we noticed expression heterogeneity in non-epithelial cell subtypes in the FT, including T/NK3, P/V3, ST2, and ST5 (Figure 2C). All ST cells in the FT (ST1–ST5) were characterized by *COL1A1* and *PDFGRA* expression. In the stroma cluster, the ST2 and ST5 subclusters expressed *DCN*, which is important for collagen assembly and as an inhibitor of angiogenesis and tumorigenesis, and *PRELP* through all three anatomic regions. ST5 cells in the isthmus and ampulla express *CD34*, *SLPI*, *C3*, *CFD*, *SFRP2*, and *SCARA5*, and these are reduced in the fimbriae, where they only express *GASK1B*. The gene expression pattern of pericytes, SM, and EN cells was mostly unchanged across all anatomic sites (Figure 2C).

Finally, we performed immunohistochemistry staining in the isthmus/ampulla/fimbriae and ovary of our patients to verify the presence of select cell types identified by scRNA-seq (Figure S2A). The staining confirmed the canonical gene expression for each cell type and anatomic region on the protein level. Vimentin was expressed in ST and epithelial cells. Epithelial cell adhesion molecule (EPCAM) was expressed primarily in the ampulla and fimbria epithelial cells and only minimally expressed in the isthmus. We also showed PAX8 protein expression in SE cells and FOXJ1 protein expression in CE cells in all 3 regions of the FT. CD45 and low levels of CD68 expression were seen in some cells in all regions of the FT and ovary (Figure S2A).

Contextualizing scRNA-seq results with genome-wide association studies (GWASs)

Gene expression measurements at single-cell resolution in the female reproductive system provide unique opportunities to pinpoint gynecological disease associations with specific cells.[14] We examined 83 putative risk genes (Table S7) related to disease-causing variants, identified from GWASs, of 8 gynecological diseases. These diseases, which include several carcinomas and endometriosis, manifest and likely originate in the FT or ovary. Ovarian cancer precursor lesions initiate premenopausally[15,16] but substantially affect postmenopausal women. We included endometriosis because it sometimes persists into menopause and can be a precursor for endometrioid and clear-cell ovarian cancer.[17] We found 65 of 83 putative risk genes expressed in at least one cell type in the FT and 64 of 83 in the ovary (Figures 3A and 3B). Not surprisingly, most risk-associated genes only manifest high expression in 1 or 2 cell types, and their expression patterns vary in the FT and ovary. Normal CE and SE cells expressed several serous high-grade ovarian cancer-related genes,[11] including keratins (*KRT17* and *KRT23*) and metabolism-related (*ALDH1A1* and *ALDH3B2),* immune-related (*HLA-DQA1* and *HLA-DPA1*), and stemness-related (*LGR5* and *CD44*) genes (Figure S3B). Surprisingly, only *MSI2,* a stemness gene expressed in high-grade ovarian cancer, showed expression in the secretory and ciliated cells of the FT (Figure 3A and Figure S3A). We discovered expression of high-grade serous ovarian cancer-associated genes in benign cell types in the FT. CE cells in all three anatomic regions of the FT highly expressed *STK33*, *TACC2*, *TTLL10*, *ADGB*, *MSI2*, and *CCDC170* (Figure 3A). These genes were not represented in SE cells, which are currently thought to be the cells of origin for high-grade serous ovarian cancer, suggesting a contribution from CE cells to the pathogenesis of the disease.[18]

The mucinous carcinoma-associated gene *CCDC80*, a known tumor suppressor in ovarian cancer[19,20] expressed in a subset of ST cells (ST2 and ST5) in the FT (Figure 3A), was confirmed using FISH (Figure 3C). The endometriosis-associated genes *COL12A1*, *GPNMB*, *BSG*, and *SEPTIN7* show moderate to high expression in ST cells in the FT (Figure 3A) but in different subsets. They also manifest high expression in various non-IM, non-epithelial cell types in the ovary: *COL12A1* in several ST compartments, *GPNMB* and *BSG* in SM cells, and *SEPTIN7* in PE cells (Figure 3B). This is particularly interesting because endometriosis is thought to arise from displaced endometrial cells and not ovarian ST cells.[21]

In addition to cell type- and tissue site-specific differences in the ovary and FT, there were significant differences in the expression patterns of GWAS genes between individual donors. Most major cell types had a unique expression signature (Figure S3A). Expression patterns in most cell subclusters were consistent in that the same set of GWAS genes was expressed in each woman, albeit to various levels (e.g., FT: P/V1/2/3, T/NK1/2/3, ST1/3, ST2/5; ovary: ST1/2/3/4/5/6/7/8, PV1/2, IM1/2). There were, however, a few notable exceptions where at least one woman expressed a distinct set of GWAS genes (FT: EN1/2, ST4; ovary: ST9/10, EN, LE). D3 and D5 expressed a relatively higher number of ovarian cancer-associated genes in the FT. In the ovaries of D3 and D5 (Figure S3A), ST9 was the subcluster expressing the most ovarian cancer-associated genes (Figure 3B). These analyses yield an expression map of risk genes in a cell type-specific and tissue site-specific fashion, providing hypotheses for the cell of origin of gynecological disease.

The ovary and the FT are hormone-responsive organs, but the current clinical thinking is that, when a woman is a few years into menopause, they are “non-functional.” To determine whether the postmenopausal FT and ovary express hormone receptors that circulating hormones can potentially activate, we systematically analyzed the expression of 63 receptors (Table S8) in the different cells of the FT and ovary and found that 60 and 59 receptors, respectively, are expressed by at least one cell type (Figure S3C). The expression of several receptors involved in metabolic regulation of FT cells (e.g., the adiponectin, insulin, and gastro-inhibitory polypeptide receptors) suggests that FT cells are metabolically active and have the receptors to respond to systemic hormonal changes. CE cells express the adiponectin, estrogen, insulin, and oxytocin receptors. All ST cells in the FT express progesterone receptors (PGR and PGRMC1) and the androgen receptor (AR), whereas these receptors are absent in the ovary (only ST9 has some PGR expression). The estrogen receptor was expressed in all ST cells of the FT but not in ST cells in the ovary (Figure S3C).

Although few cells stained for estrogen receptors and PGRs in the ovaries, as expected in postmenopause, it was intriguing to find strong immunohistochemistry staining for estrogen and PGRs in epithelial and ST cells of the isthmus/ampulla/fimbriae (Figure S3D). We then established short-term primary human cultures of ST and epithelial cells from postmenopausal FT and ovarian ST cells and found that the FT ST and epithelial cells had high ESR1 and PGR RNA expression, as detected by qRT-PCR (Figure S3E).

Ligand-receptor interactions between different cell types in the FT and ovary

To understand the interactions between different cell populations and how they jointly create the FT and ovary microenvironments, we inferred ligand-receptor interactions across all cell types in various anatomic sites using scRNA-seq as input for the CellPhoneDB software package (Figure 4; Table S9).[22] In the FT, the most robust interactions were observed between ST5 and SE and EN cells across all anatomic regions (Figure S4A). We found, across all anatomic sites, strong interactions between stroma and EN cells as well as ciliated and SE cells that were driven by CD74, a chaperone receptor. CD74 regulates antigen presentation for immune responses that can bind to MP migration inhibitory factor (MIF), a cytokine inhibiting immune function by increasing the prevalence of a highly immune-

suppressive population of myeloid-derived suppressor cells (Figure 4A).[23] We discovered significant differences when comparing ligand-receptor interactions in the isthmus and ampulla with those in the fimbriae. In the fimbriae, ciliated cells secreted COPA, a protein involved in endocytosis that could potentially bind to the CD74 receptor on ciliated, EN, and ST cells. In contrast, interactions between MIF and tumor necrosis factor (TNF) receptor family members detected in the isthmus and ampulla were absent in the fimbriae (Figure 4A).

In the ovary, we found fewer receptor-ligand interactions. Of note is the interaction between ST and EN cells secreting cytokines (*CCL4* and *CCL4L2*) that bind to IM cells (Figure 4B). We show the total number of imputed ligand-receptor interactions in D3 and D5 in the isthmus/ampulla/fimbriae and ovary (Figure S4B), where interesting anatomic region- and patient-specific differences are evident. In all anatomic regions of the FT of D3, SE, ST5, EN2, and EN4 cells show the largest number of interactions among themselves and with other cells (P/V3 and T/NK3), whereas the FT of D5 showed the highest level of interactions in the isthmus only. The ovaries of D3 and D5 showed few cellular interactions, consistent with their postmenopausal state (Figure S4B).

Because the ovary and fimbriae are in direct contact (Figure 1A), we determined the interactions between epithelial cells (SE and CE) in the FT and the different cell types in the ovary. We found potentially strong interactions between EN and ST (ST9/10) cells in the ovary with SE cells in the FT (Figures 4C and S4C). These interactions were driven by receptor-ligand pairs that play important roles in the epithelial-to-mesenchymal transition, including *PDGFR*, *FGFR*, and *CCL4* (Figure 4D). CCL4, potentially secreted by IM cells, binds to the SLC7A1 receptor expressed on CE and SE cells. SLC7A1 is important for glucose and amino acid transport across the plasma membrane (Figure 4D).

The women participating in this study represent an aging population (55 years and above), which is why we examined genomic signatures related to aging and senescence in our samples (Table S7). Senescent cells can cause tissue damage by secreting high levels of inflammatory cytokines and growth factors as part of the senescence-associated secretory phenotype (SASP).[24] We see expression of several SASP-associated genes, such as *SERPINE1*, *TIMP1*, *TIMP2*, and *IGFBP2/3/4* in FT and ovarian ST cells (many clusters) and *VEGFA*, *FGF7*, and *EGFR* in FT stroma (Figures 4E and S4D). We also note expression of several *CCL* and *CXCL* genes in IM cells from the ovary and MPs in the FT, potentially undoing some of the deleterious effects of senescence (Figures 4E and S4D). As with the scRNA-seq results, we saw significant variability between different donors in the FT and ovary (Figures S4B and S4C).

Chromatin accessibility analysis of the postmenopausal FT and ovary

scATAC-seq (10x Genomics) was performed on a subset of donors to match their scRNA-seq data. A portion of cells harvested from the FT and ovary were reserved for scRNA-seq, and the remaining cells underwent nuclei preparation and transposition treatment for scATAC-seq. Cells from the isthmus/ampulla/fimbriae from five women (D3, D4, D5, D6, and D8) were processed separately and integrated *in silico*. A total of 41,515 cells passed our quality control (QC) criteria for scATAC-seq.[25] For each individual sample, we

integrated scATAC-seq and scRNA-seq using label transfer.[26–28] When both data types were available for any given donor, we used the cluster information obtained from scRNA-seq as a reference and explicitly searched for the best-matched cluster for every single cell in scATAC-seq. In total, we identified 40,803 cells from the FT (Figure 5A) from scATAC-seq with matched scRNA-seq compartments. Table S10 shows label transfers between scRNA-seq and scATAC-seq standalone clusters. The majority of scRNA-seq and scATAC-seq clusters matched well, confirming the high quality of both datasets. Then accessibility matrices constructed at gene levels were integrated across samples using Harmony[29] and piped into the downstream analysis. We identified 25 clusters by unsupervised clustering, which could be further classified into the same 11 major cell types seen in scRNA-seq analysis (Figure S1B) based on chromatin accessibility (scATAC-seq) matched to cell type labels (scRNA-seq) (Figure 5A). Similarly, we performed scATAC-seq on ovaries obtained from three donors (D3, D5, and D8). The same QC, integration, and clustering procedures used for FT yielded 18,315 cells that could be grouped into 13 cell clusters that belong to five major cell types: ST, perivascular, EN, SM, and IM cells (Figure 5B).

We identified subclusters for several cell types in the FT that could not be differentiated by gene expression but were separated by measuring chromatin accessibility. For example, in the FT, EN1 could be further resolved into the three subclusters EN1–1, EN1–2, and EN1–3; SE cells could be resolved into subclusters SE-1 and SE-2; and P/V1 cells could be resolved into P/V1–1 and P/V1–2 by scATAC-seq (Figure 5A). P/V3 are in close proximity to ST cells, consistent with their similar gene expression.[30] EN3/4, P/V3, ST4, and T/NK3 in the FT and ST6/8/10 and lymphatic epithelial cell types in the ovary that were identified by scRNA-seq (Figures 1B and 1E) could not be detected by scATAC-seq (Figures 5A and 5B). This could be due to the similarity of these cell types regarding chromatin accessibility, differences in the number of cells profiled, or inherent limitations of the method because the percentages of cells for these subtypes were small in scRNA-seq (Figures 1F and 1G; Table S5). The percentages of identified subtypes in scATAC-seq also vary among donors (Figures 5C and 5D; Table S6).

We performed meta-gene analysis to characterize the global accessibility of different cell types by examining transcription start site (TSS) enrichment scores from +/−1000 bp of TSS regions across all genes. We observed that P/V3 and P/V2 are among the cell types with highest accessibility, SE and CE among the least accessible, and P/V1 cells are in between. This may suggest that, in menopause, a subset of pericytes undergo active regulation, whereas epithelial cells are less active. We observed that the patterns in the isthmus and ampulla are similar compared with that in fimbriae, where P/V1, CE, and SE all show lower accessibility (Figure S5A).

To fully characterize the regulatory landscape in the FT and ovary, we estimated the activities of 870 transcription factors (TFs) listed in the cisBP database[31] in a cell type-specific fashion (Figures 5E and 5F; Table S11). In the ovary, we found ST5, SM, PE2, and IM cells to be the cell types with highest number of enriched TFs (Figure 5F). The ETS like-1 (ELK), E74-like factor (ELF) and specificity protein 1 (SP) TF families are enriched in EN and IM cells, and the Early B-cell factors (EBF) and Myeloid elf-1 like factor (MEF) families are enriched in PE1 and PE2 (Figure 5F). Most of the ST cells in the

ovary show less TF enrichment, except for ST5, which shows relatively higher enrichment in the Guanine-adenosine-thymine-adenosine (GATA), Forkhead box (FOX), and T-cell factor (TCF) families. The Zing finger and broad-complex, tramtrack and bric a brac (ZBTB) and Yin Yang (YY) families are enriched in IM cells, which is consistent with ZBTB7B's and ZBTB7A's roles in regulating the development and/or differentiation of conventional CD4/CD8 αβ+ T cells and the role of YY1 in regulating broad general processes throughout all stages of B cell differentiation.[32,33]

FOXL2 is essential for embryogenesis, cell differentiation, and tumorigenesis. The highly conserved nature of this gene and its limited expression, predominantly in the ovary, suggest that it is a key factor throughout ovarian development. We detected high *FOXL2* expression (↑) and *SOX9* supression (↓) in several ST clusters in the FT (ST1/3/4) (Figure S5B). This pattern is reversed in SE and CE cells (*FOXL2*↓ and *SOX9*↑) of the FT (Figure S5B). Most FOX TF family members[34] show enrichment in the ovary (Figure 5F). SOX9 is depleted in ST cells in the ovary (Figure S5F).

Ablation of FOXL2 in the adult mouse ovary causes immediate induction of the TF SOX9, leading to ovary-to-testis *trans*-differentiation. We observe a similar pattern of high *FOXL2* and low *SOX9* expression in several ST clusters of the FT when reviewing the browser track plots of FOXL2 and SOX9 accessibility and expression (from scATAC-seq and scRNA-seq data, respectively) for each cell type and anatomic location (Figures S5C–S5E). In SE and CE cells of the FT, *SOX9* shows a strong chromatin accessibility signal, and *FOXL2* shows no signal. *FOXL2* chromatin accessibility is found in ST2/5 in the fimbriae but is absent in the isthmus and ampulla. *FOXL2* is expressed across isthmus/ampulla/fimbriae for ST1/3/4. This is yet another instance of expression patterns differing in ST2/5 compared with ST1/3/4 in the FT as a whole (Figure S1C) and by anatomic location (Figures S5C–S5E).

Identification of cell type- and location-specific regulatory elements using scATAC-seq

The chromatin landscape in the FT displays similar patterns in the isthmus, ampulla, and fimbriae (Figure 6A). However, the TF motif analysis revealed that, although regulation patterns across cell types are almost identical in the isthmus and ampulla, they are strikingly different in the fimbriae (Figures 6B and 6C). For example, SE-1 and SE-2 show more motif enrichment in the isthmus and ampulla than in the fimbriae. MA cells show more enriched TFs in the fimbriae compared with those in the isthmus and ampulla (Figure 6B). In contrast, IM cells, including B/P, T/NK, and MP cells, exhibit similar patterns across all 3 anatomic regions, suggesting that the entire FT may respond similarly to immune stimuli (Figure 6B). Equally important, other cell types in the isthmus and ampulla (SM and EN2) and ST1–ST3 cells across all FT regions display few enriched TFs (Figures 6B and 6C). Surprisingly, CE and SE cells show lower TF activity of Sry-type HMG box (SOX), Signal transducers and activators oftranscription (STAT), and ZBTB TFs in the fimbriae, whereas the FOX TF family is high in CE cells across all 3 anatomic regions of the FT. In respect to EN cells, we observed an increased signal in SOX family members from the isthmus/ampulla to fimbriae. The EN1–1/2 subclusters are characterized by their differences in enrichment of pro-inflammatory STAT TFs (high in fimbriae), which play a role in EN cell dysfunction during aging.[35] EN1–1 and EN1–2, both derived from the same EN1 cluster

in scRNA-seq (Figure 1B) via label transfer, must therefore have similar gene expression. Using scATAC-seq, we found that, in fimbriae, the EN1–2 subclusters have high EFL2 and TCF7L1 enrichment, whereas EN1–1 has high YY1 and YY2 enrichment. These findings suggest that EN cells express similar genes but may be regulated by different TFs (Figure S6A). For ETV2, TF enrichment progressively decreases from the isthmus to fimbriae in EN1–3 and increases from isthmus to fimbriae in EN1–1 (Figure S6A).

Known Epithelial-mesenchymal transition (EMT)-related TFs, including BACH1 (Figure 6C), SNAI1, SNAI2, ZEB1, and TWIST1 (Figure S6B), show enrichment in SE but not in ST cells, suggesting EMT-related TF activity specifically in FT epithelial cells. The JUN/FOS family of TFs shows enrichment in ST5 and SE cells (Figure S6B), where different isoforms of JUN and FOS proteins are enriched in epithelial (SE-1) and ST cells (ST5). SE-1 expressed FOS/JUND, which has a known inhibitory transcriptional function.[36,37] The TF RUNX3, which plays a critical role in differentiation of premenopausal FT,[7] was not expressed in CS and SE cells but showed increased enrichment in T/NK cells.

We then overlapped cisBP TFs with our curated list of GWAS genes (Table S7) and identified 6 GWAS-associated TFs, including ARID3B, BRCA1, GLI3, MECOM, PBX3, and PPARA. For each TF, we examined the gene activity score, which measures accessibility of the TSS region of a given gene. Gene activity scores were similar in the isthmus and ampulla but strikingly different in the fimbriae. In the isthmus and ampulla, most TFs show high activity in CE and SE cells but are less active in the other cell types. In contrast, in the fimbriae, TF gene activity is more robust in most non-epithelial cells (EN and ST2/3/5) (Figure 6D). There are several cell types showing major differences in TF gene activity in the fimbriae (MPs ↑, EN ↑, CE ↓, and SE ↓). These differences were not evident when analyzing TFs using scRNA-seq data and only became evident when inspecting cluster-specific TF activities identified from scATAC-seq data.

DISCUSSION

The FT and ovary, which are crucial to the female reproductive system, are thought to have little physiologic function after menopause. However, these organs are often the origin of diseases that persist through menopause (e.g., endometriosis) or newly develop (benign or malignant tumors) later in life. Without an appreciation of the healthy state of an organ, it is difficult to understand any pathological condition, and therapies are most effective when they address the underlying changes from the normal to the diseased state.

With this in mind, we set out to systematically characterize the gene expression and regulatory landscape of all cell types in the human postmenopausal FT and ovary at single-cell resolution to develop a resource that could be a starting point for all scientists studying female well-being and disease. The different cell types we identified in the FT overlapped almost entirely with a recent report on one postmenopausal FT.[7] Because the histologic appearance of the FT close to the uterus and at the fimbrial end is so different, we separately examined several anatomic regions of the FT. In all 11 cell types, there was little change in gene expression between the three anatomic areas of the FT. However, there

were remarkable differences in chromatin accessibility between the fimbriated end of the FT compared with the isthmus and ampulla. Several cell types in the fimbriae showed strong enhancer activity that included MP, EN, perivascular, and some ST cell types. EN cells in the fimbriae showed increased accessibility to the SOX TF family, known to activate the endothelium.[38] Because the SOX TF family is involved in tissue repair/regeneration and EN mesenchymal transition, upregulation in fimbriae is probably a reaction to chronic exposure of the fimbriae to the peritoneal cavity fluid or aging of the FT. Ciliated and SE cell types that have been implicated previously in disease etiology showed limited chromatin accessibility to the STAT and ZBTB family of TFs in the fimbriae, indicating resting/senescent epithelium.[39] Senescent cells can cause tissue damage by secreting high levels of inflammatory cytokines and growth factors as part of the SASP.[24] SASP-associated genes, such as *VEGFA*, *FGF7*, and *EGFR*, are expressed in FT stroma, and others, such as *SERPINE1*, *TIMP1*, *TIMP2*, and *IGFBP2/3/4* are expressed in FT and ovarian ST cells (several clusters).

In contrast, immune cells throughout all anatomic regions of the FT as well as the ovary remain transcriptionally active and express antigens and cytokines, indicating that both organs are not immunologically inert. We also noted expression of several *CCL* and *CXCL* genes in immune cells from the FT (MPs) and ovary, potentially undoing some of the deleterious effects of senescence and aging. We did not find any of the subclusters reported by Ulrich et al.[6] in their elegant study of premenopausal FTs. Nor did we find the subclusters detected by Dinh et al.[7] in the premenopausal FT. Using scRNA-seq, we found just one type of CE and SE cell each, but with scATAC-seq, we could resolve SE cells into SE-1 cells, which are accessible to multiple FOS/JUN heterodimers and EMT-regulating TFs, and SE-2 cells, which have low occupancy for most of these TFs. With menopause, the FT epithelium loses the sophisticated subdifferentiation of epithelial cells probably required to perform its reproductive functions.

For our study, we used fresh tissue from healthy postmenopausal women that was apparently normal on microscopic examination and expressed clinically established immunohistochemical markers. We learned that the concept of “normal” tissue is relative; although all cell types were represented in every patient, there was wide variation in gene expression between patients, consistent with reports of “normal” lung[14] and kidney[26] tissue. Even when all cells of a “normal” cell type had the same gene expression, we found that subclusters varied in their transcriptional regulatory patterns. For example, scATAC-seq allowed identification of three EN subclusters (EN1–1/2/3) in the FT, which were each regulated by a different set of TFs but showed similar gene expression. This observation could explain the remarkable adaptability of “normal” cells to stressors in the local microenvironment, highlighting the startling self-healing potential of utilizing redundant regulatory pathways. Our data suggest that integration of scRNA-seq and scATAC-seq is essential for deciphering the cellular complexity of tissues, which would not be possible with either of the assays alone. A limitation of our integration was our inability to confirm gene expression levels corresponding to TF activity for cellular subtypes identified from scATAC-seq alone. This limitation can be overcome in future studies by using recent multi-omics assays that simultaneously measure gene expression and chromatin accessibility from the same cell.

When correlating our scRNA-seq results in the FT with endometriosis-associated[40] risk genes, we identified *GPNB*, a gene implicated in the inflammatory response, in ST subclusters ST2/5 and *BSG*, an immunoglobulin family member frequently detected in ectopic endometrial tissue, in ST1/3/5.[41] *BSG*, also known as EMMPRIN or CD147, promotes cell proliferation by blocking apoptosis and upregulating mitogen-activated protein kinase (MAPK) signaling in human endometrial epithelial cells.[42] In the ovary, *EIF3H*, a translation initiation factor implicated in endometriosis, was expressed in 6 ST subtypes. It is intriguing that most of the candidate risk genes found in endometriosis are expressed in ST cells and may suggest that the microenvironment plays a role in sustaining endometriosis.

Several ovarian cancer risk genes implicated by GWASs were also expressed in ST cell populations in the FT. ST clusters ST2/5 expressed *CCDC80*,[19] which is part of a tumor microenvironment gene signature derived from the ovarian cancer-related The cancer genome atlas (TCGA) data.[43] Surprisingly, most GWAS-derived risk genes in the normal postmenopausal FT were not expressed in secretory cells, which have been posited as possible ovarian cancer cells of origin.[44] This could be also explained by the fact that ovarian cancer precursors probably initiate decades before menopause.[15] GWAS genes were found in CE cells (*TTLL10*, *MECOM*, *TACC2*, *CCDC170*, *MSI2*, *BRCA1*, *STK33*, *ADGB*, and *CMIP*).

We also present the first scRNA-seq and ATAC-seq atlas of the human postmenopausal ovary. Most cells in the postmenopausal ovary are ST cells, but there is also a substantial number of EN cells, consistent with the very rich blood supply to the ovary. There are few IM cells in the postmenopausal ovary and, unlike the ovaries of aged peri-menopausal non-human primates,[45] no follicles were detected, suggesting complete follicular atresia in human menopause. The human postmenopausal ovary had a much higher variation in ST gene expression than that of the monkeys, but in contrast to the peri-menopausal monkey ovary, very few genes were associated with senescence or DNA oxidation. In general, the ST cells in the postmenopausal ovary are not very transcriptionally active; however, the ST5 cluster retains marked accessibility for all FOX and GATA TF family members compared with the other ST subclusters. Based on the ATAC-seq data, EN, SM, and IM cells in the postmenopausal ovary have high chromatin accessibility, so by no means should the ovary be considered a quiescent organ, especially given the strong expression of several hormone receptors potentially bound by circulating hormones (e.g., leptin, androgen, prostaglandin receptors, etc.). It is fascinating that, in the postmenopausal setting, ovarian cells have almost no estrogen receptor expression, whereas all FT ST cells have high estrogen receptor and PGR expression. Unopposed estrogen production during menopause (e.g., from adipose tissue) might cause mutagenic effects in the tube, as described for the postmenopausal endometrium, in which estrogen contributes to the transformation of the resting epithelium.[46] The fimbrial end of the FT and the ovary are next to each other and depend on close anatomic and functional interactions to transfer the oocyte during ovulation from the ovary to the FT. Our results indicate that the FT epithelial cell types (CE and SE) and ovarian ST and IM cells may interact directly through complementary ligand-receptor expression. These findings provide the basis for follow-up studies using high-content spatial transcriptomics/proteomics imaging.

There are several major caveats to motif-based TF analysis using scATAC-seq data. (1) High redundancy across motifs, particularly in families of related factors, can make it difficult to pin down the particular TF that is active in the family. (2) Many TFs with poor or absent motifs, resulting in absence of enriched motifs, could mean that the important TFs for that cell type are absent from the reference database. Expression in the same cellular compartments might help prioritize the active TFs if we assume that active expression of a TF is a prerequisite for its function. Because our scRNA data are collected from cells and our scATAC data are collected from nuclei, this strategy may have limited efficacy in our study. We constrained the motif analysis to expressed TFs to see whether this will alter our findings (expressed TFs are defined as those that have an average expression greater than 0 from paired scRNA-seq data in all cell types). We identified 330 expressed TFs across all anatomic regions of the FT and 295 expressed TFs in the ovary. Overall patterns of motif enrichment analysis across the isthmus (I), ampulla (A), and fimbria (F) remain unchanged; i.e., the motif enrichment in I and A is almost identical but shows obvious differences from the F, particularly for cell types SE1, SE2, and CE (Figure S6C).

With this study, we focused on the postmenopausal FT and ovary and were able to characterize the largest number of FT and ovarian cells in a single integrated study to date. We characterized and integrated the regulatory and transcriptional landscape of the postmenopausal FT and ovary at single-cell resolution, providing an important reference dataset to study reproductive physiology and disease. The challenge that remains is integration and translation of this information into functional studies *in vivo* to ultimately provide effective therapies for previously intractable disease states.

Limitations of the study

We were only able to perform scATAC-seq analysis on a subset of donors smaller than the group used for our scRNA-seq experiments. This means that fewer cells were sampled by scATAC-seq overall, and, as a result, we were not able to resolve all cell types identified by scRNA-seq.

As mentioned earlier, scATAC- and scRNA-seq are from similar cells but not actually from the same cell. This was a confounding factor in this study. We posit that newer single-cell genomics assays will allow a more straightforward interpretation because we will have chromatin accessibility and gene expression profiles from the same cell.

Chromatin accessibility is a necessary but not a sufficient indicator of gene expression. Our TF analysis assumes that all TFs from open chromatin regions are active; however, this assumption may not hold, especially for chromatin regions that are rich in TF activity. Conversely, TFs with poor, absent, or still unknown motifs may be missing from our analysis.

Finally, all scRNA-seq and scATAC-seq analyses are descriptive and reflective of gene expression at one moment in time. Although our results suggest possible cellular functions, they have not been validated with functional experiments. We set out to establish a human cell atlas of the “normal” postmenopausal FT and ovary. We came to understand that

"normal" is not uniform but involves a range of gene expressions for each cell type and cellular heterogeneity associated with the absence of clinically manifested disease.

STAR★METHODS

RESOURCE AVAILABILITY

Lead contact—Further information and requests for resources should be directed to and will be fulfilled by the lead contact, Ernst Lengyel (elengyel@uchicago.edu).

Materials availability—Requests for resources and reagents should be directed to and will be fulfilled by the lead contact, Ernst Lengyel (elengyel@uchicago.edu).

Data and code availability—Processed and de-identified human single-cell RNA and ATAC sequencing data have been deposited at Cellxgene under the following URL: https://cellxgene.cziscience.com/collections/d36ca85c-3e8b-444c-ba3e-a645040c6185and raw data has been deposited at the European Genome-Phenome Archive (EGA) with the accession number EGAS00001006780. Both data sets will be publicly available as of the date of publication. The link to the data is listed in the key resource table.

This paper does not report original code.

Any additional information required to reanalyze the data reported in this paper is available from the lead contact upon request.

EXPERIMENTAL MODEL AND SUBJECT DETAILS

Human subjects and tissue acquisition—Fallopian tube and ovary samples were collected from postmenopausal female patients who underwent elective surgical hysterectomy for benign indications (vaginal prolapse, incontinence) and were having these tissues removed as part of their normal surgical procedure performed at The University of Chicago Medical Center (Table S1). Postmenopause was defined as the absence of a menstrual cycle for greater than two years and/or absent menses with accompanying symptoms of menopause. Signed informed consent was obtained from the patient prior to the elective procedure. All procedures involving human samples were conducted in accordance with the Institutional Review Board at the University of Chicago.

METHOD DETAILS

Immunohistochemistry—Five μm sections of formalin-fixed paraffin-embedded tissues from postmenopausal women were sectioned and stained with hematoxylin and eosin or with commercially available antibodies by the Human Tissue Resource Center at the University of Chicago using the Leica Bond RX automated stainer (Leica Biosystems). All slides were reviewed by gynecologic pathologists. The following antibodies were used for immunohistochemistry: FOXJ1 at 1:500, CD68 at 1:200, CD45 at 1:100, pan cytokeratin at 1:200, vimentin at 1:2000, PR at 1:300, ER at1:180, PAX8 at 1:1000, EPCAM at 1:75, WT1 at 1:400, CK7 at 1:1000.

Tissue dissociation—Tissue specimens from eight patients were collected and processed (Table S1). The tissue was removed surgically and processed within 20 minutes after the tissue was amputated from its surrounding tissue and blood supply.[52] The three anatomic regions (isthmus, ampulla, and fimbriae) were further dissected and dissociated independently into single cell suspensions for higher anatomical resolution.

100 mg of ovarian tissue and 2–3 mm cross-sections of each fallopian tube segment (100 mg each of isthmus, ampulla, and fimbriae) were digested independently.[53] Each tissue slice was rinsed with a fetal-bovine serum enriched DMEM to remove blood and mucus and surrounding parametrial tissue was trimmed. The dissociation was a two-stage protocol separating each tissue into epithelial and fibroblast components with an initial epithelial digestion with pronase (7 U/mg) in Opti-MEM at 37° for 30 minutes[54]. Epithelial cells were filtered out and the remaining stroma-fibroblast supernatant underwent second digestion with tissue DNAse I (20,000 U/mL), collagenase IV (120 U/mg), hyaluronidase (2000 U/mg) in HBSS at 37° for 30 minutes. At the end of the digestion, the epithelial and stromal-fibroblast components were combined and passed through a 70 μm filter. The cell suspension was spun at 400 rcf for 7 minutes and the cell pellet was re-suspended in DMEM+FBS. To remove remaining red blood cells from processing, red blood cell lysis solution (EasySep RBC Depletion Reagent) was used. The cells were imaged, and cell counts were obtained. During dissociation, we aimed for cell viability over 85% (assessed by Trypan blue and/or Annexin V staining) and cells of diverse morphologies (assessed by bright-field imaging) to meet QC criteria.

Fluorescent RNA *in situ* hybridization (RNAScope)—RNAscope was performed on 5 μm sections of formalin-fixed and paraffin-embedded tissues using the Leica Biosystems' BOND RX System and ACD biotech user manual (Document number: 322800-USM) for the RNAscope LS multiplex fluorescent reagent kit user manual for BDZ 11. The following probes were purchased from ACD biotech for RNAscope: DCN and CCDC80. Images were acquired using a Nikon Eclipse Ti2 microscope and processed using the Nikon software NIS-Elements.

Single cell RNA-seq—scRNA-seq was performed on 8 donors using Drop-seq (2 donors-D1, D2) and 10X Genomics (6 donors, D3 - D8 using the 10x Genomics 3′ RNA-seq assay).

Drop-seq—Drop-seq experiments were performed as previously described.[55] Briefly, cells and oligonucleotide barcode beads were loaded at concentrations of 100,000 cells/mL in PBS-BSA and 120,000 beads/mL in Drop-seq lysis buffer in 3 mL syringes. Droplets were generated using a 125-micron microfluidic device at 16 mL/hr (oil), 4 mL/hr (cells) and 4 mL/hr with ~15 minutes per collection. Following collection, drops were broken and barcoded beads with mRNA hybridized onto them were collected and washed. Barcoded cDNA attached to the beads or Single-cell Transcriptomes Attached to MicroParticles (STAMPs) were generated by reverse transcription, treated with Exonuclease I and the number of STAMPs was counted. 5000 STAMPs were aliquoted per well in a 96-well plate and the cDNA attached to the STAMPS were amplified through 15 PCR cycles. Supernatants from each well were pooled and cleaned with Ampure beads. Purified cDNA was quantified using Qubit 3.0 and 450–650 pg of each sample was used as input

for Nextera reactions using the Nextera XT DNA kit (12 cycles). Tagmented libraries were quantified using Agilent BioAnalyzer High sensitivity chip before submission for sequencing on Illumina's NextSeq 500, using 75 cycle v3 kits. Paired end sequencing was performed with 20 bp for Read 1 and 60–64 bp for Read2 using a custom Read1 primer, and 5% Illumina PhiX Control v3.

10x genomics 3′ scRNA-seq—Single-cell suspensions were transported to the lab in warmed media to preserve viability. Cells were washed once with PBS + 0.4% BSA and resuspended in PBS + 0.4% BSA to achieve a target cell count of 700–1200 cells/μL and loaded according to the Chromium Next GEM protocols. Single-cell suspensions from each sample were loaded onto the fluidic chip at X cells/uL and were constructed into barcoded 3′ scRNA-seq libraries using the Chromium Next GEM kit, v3 targeting 8,000 cells/sample, except for two samples from the isthmus (D4 and D5) that had a low number of cells and only 2000 cells were targeted. Sequencing libraries were constructed following 10x Genomics protocols with 15 amplification cycles. Bioanalyzer 2100 traces were used to evaluate cDNA and final sequencing libraries. The libraries were sequenced through the University of Chicago core facilities using a PE75 run on the Illumina NextSeq 500 or NovaSeq platforms. Libraries were sequenced at 30,000–50,000 reads per cell according to the manufacturer's recommendations.

scRNA-seq data analysis—The original raw BCL (binary base call) sequencing data were converted and demultiplexed into FASTQ files by a wrapper function, *cellranger mkfastq*, from Cell Ranger software[56] developed by 10x Genomics. Then the raw sequencing reads were aligned to the human reference genome hg38 and then filtered and quantified as UMI counts using barcode information via *cellranger count*. We further applied the following QC criteria to the UMI count matrix using an in-house pipeline: 1) we require cells expressing at least 200 gene features and each gene feature present in at least 3 cells; 2) we remove doublets and triplets identified by *DoubletDecon*[48]; 3) cells with ≥20% mitochondrial contents were filtered out as poor-quality cells with low viability. Each UMI count matrix, with cells from a certain anatomical site of a donor, is log-normalized using a procedure[57] implemented with *Seurat*[49] function *NormalizeData* and *FindVariableFeatures*. Cells from different samples were integrated using *Seurat* function *FindIntegrationAnchors*,[58] where top 2,000 highly variable gene features expressed across cells were used as anchors for pairwise sample integration. Prior to dimensionality reduction, a linear transformation scaling procedure was applied to remove unwanted variations. We performed dimensionality reduction using both PCA and UMAP. Shared nearest-neighbor (SNN) graph was constructed for graph-based clustering via *Seurat* function *FindNeighbors* and *FindClusters* correspondingly, at resolution of 0.5 for a relatively dense clustering. Cell clusters obtained from unsupervised learning (top 100 differentially expressed genes in the FT and ovary are listed in Tables S2 and S4) were further manually annotated using canonical markers of different cell types curated from the literature (Table S3). Sub-clustering of immune NK/T cells was performed by HIPPO,[8] a method solving cellular heterogeneity using zero proportions instead of gene variance. The raw UMI counts of selected cells were input to HIPPO for sub-clustering analysis, with the number of clusters specified 2 times higher than the number of clusters originally identified

from Seurat. To avoid early stop before the specified number of clusters, we used a z-score threshold of 1 with default outlier proportion of 0.001%. Obtained sub-clusters are further characterized using a set of additional immune markers (Table S3).

Our scRNA-seq data was compared with datasets of normal epithelial cells by Hu, et al., *Cancer Cell* 2020[11] and one postmenopausal patient from Dinh, et al., *Cell Reports*, 2021.[7]

GWAS analysis—We curated a list of 84 genes that contained disease-causal variants for 8 disease categories from public GWAS databases. We checked the expression levels of these genes in our scRNA-seq data. Among these, 6 genes (GPC5, CALHM3, PA2G4P2, SNTG1, KRT18P55, PKD1L1) were barely expressed in all cell types and were removed from further exploration. This resulted in a total of 78 GWAS genes (Table S7) for downstream comparisons and display.

Ligand-receptor analysis using CellPhoneDB—The normalized gene expression data were used as the input for CellPhoneDB. The ligand-receptor interaction analysis utilizes CellPhoneDB function curated by CellPhoneDB database v2.0.0. Significant ($p < 0.05$) receptor - ligand interactions between any two cell types in different anatomy sites in fallopian tube were displayed (Table S9). Similar analyses were conducted and displayed for interactions of cell types in ovary, and interactions between CE and SE in fimbriae and cell types in ovary.[22]

Single cell ATAC-seq—Fresh single-cell suspensions were lysed on ice for 4 minutes to obtain intact nuclei. The nuclei were tagmented at 37°C for 1 hr according to standard protocol for the Chromium Next GEM kits to generate scATAC-seq libraries with 6,000–8,000 nuclei per sample. All downstream procedures were performed following standard manufacturer's protocols. Agilent 2100 Bioanalyzer traces were used to evaluate final library quality. The libraries were sequenced following 10x Genomics guidelines on Illumina NextSeq 500 and NovaSeq platforms through the University of Chicago Core Facility. Libraries were sequenced at 25,000–30,000 read pairs per nucleus according to the manufacturer's recommendations.

Processing and quality control of scATAC-seq data—ScATAC-seq data was analyzed using the scATAC-pro workflow.[25] Raw sequencing data from each sample were aligned to human hg38 reference genome using *cellranger ATAC 1.2*. R Seurat v4.0 [54,56] and *Signac v1.4.0*[50] were used for further analysis. High quality cells, defined as cells with peak region fragments >3000, peak region fragments <20000, % of reads in peaks >15, blacklist ratio <0.05, nucleosome signal <5 and TSS enrichment >2, were retained for normalization using term-frequency inverse-document-frequency (TFIDF). The Seurat objects from each sample (after label transfer from scRNA-Seq) were merged based on the common peak set which was created by merging peaks from all the datasets. Dimensional reduction was performed via singular value decomposition (SVD) of the TFIDF matrix and UMAP. Batch effects across samples were corrected by *Harmony*[29] using *RunHarmony* function on the first 30 latent semantic indexing (LSI) components, excluding the first one because it was highly correlated with the sequencing depth. Finally, gene activity scores were estimated using *Seurat* function *GeneActivity*.[49] Data corrected by *Harmony* were

used for unsupervised clustering analysis using *FindNeighbor and FindClusters* functions in *Seurat*.[49]

Integration of scRNA-seq and scATAC-seq datasets—To obtain cell types of scATAC-seq data, cells from the matched scRNA-seq analysis were used as a reference dataset to predict cell types in the scATAC-seq. This prediction used the variable features of the scRNA-seq data as reference, and the gene activity matrix generated using Seurat's *GeneActivity*[49] from scATAC-Seq data as the query data. Transfer anchors were learned using FindTransferAnchors[49] and cell type labels were predicted using *TransferData*[49] with the scATAC-seq LSI reduction as *weight.reduction* input. Specifically, we assign each cell in the scATAC-seq with a cell type (subcluster) identity from the matching scRNA-seq data based on the first 30 LSI components corrected by *Harmony*, excluding the first one. Only cells with the prediction score, denoted by *prediction.score.max* that quantifies the uncertainty with predicted annotations, larger than 0.5 were kept for further analysis. Cell clusters transferred from scRNA-seq were further separated into sub-clusters if supported by unsupervised clustering analysis using scATAC-seq data alone. The label transfer procedure was performed for each individual patient separately (Table S10).

Transcription factor motif analysis—Transcription factor activities (Table S11) were estimated from *Harmony* integrated scATAC-seq data using chromVAR v3.14.[51] TFs and their binding motifs listed in human_pwms_v2(cisBP)[31] database was used as another input to chromVAR for positional weight matrix calculation. RunChromVAR[51] in Signac was applied to calculate the cell type-specific TF activities and differential activities among cell types were computed with *FindMarkers* with Bonferroni-adjusted p-values < 0.05.[26,27] The total number of motifs in cisBP database is 870, while there are only 869 motifs detectable in fimbriae and since we ordered the heatmaps according to fimbriae, there are 869 motifs shown in heatmaps. To obtain a more comprehensive profiling for JUN/FOS family motifs we also checked JASPAR database,[47] which in total contains 633 motifs, within which 29 are JUN/FOS family motifs, significantly more than the collection in cisBP (8 out of 870). These JUN/FOS motifs have different splice forms resulting in different binding specificity, which were handled as binding variants and could be seen from their names (e.g., FOS::JUN(MA0099.3) and FOS::JUN(var.2) (MA1126.1)). The TF enrichment analysis of all motifs was performed for each cell type in each tissue site separately. The results were then compared and displayed.

QUANTIFICATION AND STATISTICAL ANALYSIS

The cell numbers were summarized based on cells annotation with respect to each anatomical regions. The relative cell percentage was normalized by the total number of cells with respect to each anatomical region separately. Significance includes everything with P<=0.05.

Unless stated otherwise, all quantitative data are represented as mean ± standard deviation (SD). Indicated sample sizes (n) represent biological samples. Sample sizes, statistical tests and p values are indicated in the figure legends. Statistical analysis of qPCR results were performed using GraphPad Prism 8 software. Significance was analyzed using one-way

ANOVA comparing the mean of each column with the mean of the control followed by multiple-comparison post-testing with Dunnett's method.

Supplementary Material

Refer to Web version on PubMed Central for supplementary material.

ACKNOWLEDGMENTS

We thank Dr. Mark Eckert for support and strong dedication during the initial phase of this project. We thank Gail Isenberg for help with editing the article. This work was mainly supported by the Chan Zuckerberg Initiative (to E.L., A.B., M.W., and M.C.). M.C. is supported by the NIH (R01 GM126553 and R01 HG011883), the National Science Foundation (NSF; 2016307), and the Sloan Research Fellowship Program. A.B. is supported by NIH DP2AI15 8157. E.L. is supported by R35CA264619, RO1CA211916, RO1CA237029, and the Ovarian Cancer Research Alliance. We thank the Genomics Facility, Human Tissue Resource Center, and Pritzker Nanofabrication Facility at the University of Chicago for equipment and services and Dr. Ran Zhou for help with single-cell experiments. Microfluidics devices were fabricated at The University of Chicago. Patients from The University of Chicago OB/GYN department donated tissue for this study.

REFERENCES

1. Scully RE, Young RH, and Clement PB (1998). Atlas of Tumor Pathology, Tumors of the Ovary, Maldeveloped Gonads, Fallopian Tube, and Broad Ligament, 3 Edition (Armed Force Institute of Pathology).
2. Ardighieri L, Lonardi S, Moratto D, Facchetti F, Shih IM, Vermi W, and Kurman RJ (2014). Characterization of the immune cell repertoire in the normal fallopian tube. Int. J. Gynecol. Pathol. 33, 581–591. 10.1097/PGP.0000000000000095. [PubMed: 25272297]
3. Kurnit KC, Fleming GF, and Lengyel E. (2021). Updates and new options in advanced epithelial ovarian cancer treatment. Obstet. Gynecol. 137, 108–121. 10.1097/AOG.0000000000004173. [PubMed: 33278287]
4. Soong TR, Howitt BE, Horowitz N, Nucci MR, and Crum CP (2019). The fallopian tube, "precursor escape" and narrowing the knowledge gap to the origins of high-grade serous carcinoma. Gynecol. Oncol. 152, 426–433. 10.1016/j.ygyno.2018.11.033. [PubMed: 30503267]
5. Lengyel E. (2010). Ovarian cancer development and metastasis. Am. J. Pathol. 177, 1053–1064. 10.2353/ajpath.2010.100105. [PubMed: 20651229]
6. Ulrich ND, Shen YC, Ma Q, Yang K, Hannum DF, Jones A, Machlin J, Randolph JF Jr., Smith YR, Schon SB, et al. (2022). Cellular heterogeneity of human fallopian tubes in normal and hydrosalpinx disease states identified using scRNA-seq. Dev. Cell 57, 914–929.e7. 10.1016/j.devcel.2022.02.017. [PubMed: 35320732]
7. Dinh HQ, Lin X, Abbasi F, Nameki R, Haro M, Olingy CE, Chang H, Hernandez L, Gayther SA, Wright KN, et al. (2021). Single-cell transcriptomics identifies gene expression networks driving differentiation and tumorigenesis in the human fallopian tube. Cell Rep. 35, 108978. 10.1016/j.celrep.2021.108978.
8. Kim T, and Chen M. (2021). HIPPO: Heterogeneity-Induced Pre-processing Tool. http://bioconductor.org/packages/devel/bioc/html/HIPPO.html.
9. McKinney EF, and Smith KGC (2018). Metabolic exhaustion in infection, cancer and autoimmunity. Nat. Immunol. 19, 213–221. 10.1038/s41590-018-0045-y. [PubMed: 29403049]
10. Tatone C, and Amicarelli F. (2013). The aging ovary–the poor granulosa cells. Fertil. Steril. 99, 12–17. 10.1016/j.fertnstert.2012.11.029. [PubMed: 23273984]
11. Hu Z, Artibani M, Alsaadi A, Wietek N, Morotti M, Shi T, Zhong Z, Santana Gonzalez L, El-Sahhar S, KaramiNejadRanjbar M, et al. (2020). The repertoire of serous ovarian cancer non-genetic heterogeneity revealed by single-cell sequencing of normal fallopian tube epithelial cells. Cancer Cell 37, 226–242.e7. 10.1016/j.ccell.2020.01.003. [PubMed: 32049047]

12. Shih AJ, Menzin A, Whyte J, Lovecchio J, Liew A, Khalili H, Bhuiya T, Gregersen PK, and Lee AT (2018). Identification of grade and origin specific cell populations in serous epithelial ovarian cancer by single cell RNA-seq. PLoS One 13, e0206785. 10.1371/journal.pone.0206785.

13. Lemire M, Qu C, Loo LWM, Zaidi SHE, Wang H, Berndt SI, Bézieau S, Brenner H, Campbell PT, Chan AT, et al. (2015). A genome-wide association study for colorectal cancer identifies a risk locus in 14q23.1. Hum. Genet. 134, 1249–1262. 10.1007/s00439-015-1598-6. [PubMed: 26404086]

14. Travaglini KJ, Nabhan AN, Penland L, Sinha R, Gillich A, Sit RV, Chang S, Conley SD, Mori Y, Seita J, et al. (2020). A molecular cell atlas of the human lung from single-cell RNA sequencing. Nature 587, 619–625. 10.1038/s41586-020-2922-4. [PubMed: 33208946]

15. Wu RC, Wang P, Lin SF, Zhang M, Song Q, Chu T, Wang BG, Kurman RJ, Vang R, Kinzler K, et al. (2019). Genomic landscape and evolutionary trajectories of ovarian cancer early precursor lesions. J. Pathol. 248, 41–50. 10.1002/path.5219. [PubMed: 30560554]

16. Eckert MA, Pan S, Hernandez KM, Loth RM, Andrade J, Volchenboum SL, Faber P, Montag A, Lastra R, Peter ME, et al. (2016). Genomics of ovarian cancer progression reveals diverse metastatic trajectories including intraepithelial metastasis to the fallopian tube. Cancer Discov. 6, 1342–1351. 10.1158/2159-8290.CD-16-0607. [PubMed: 27856443]

17. Pearce CL, Templeman C, Rossing MA, Lee A, Near AM, Webb PM, Nagle CM, Doherty JA, Cushing-Haugen KL, Wicklund KG, et al. (2012). Association between endometriosis and risk of histological subtypes of ovarian cancer: a pooled analysis of case-control studies. Lancet Oncol. 13, 385–394. 10.1016/S1470-2045(11)70404-1. [PubMed: 22361336]

18. Coan M, Rampioni Vinciguerra GL, Cesaratto L, Gardenal E, Bianchet R, Dassi E, Vecchione A, Baldassarre G, Spizzo R, and Nicoloso MS (2018). Exploring the role of fallopian ciliated cells in the pathogenesis of high-grade serous ovarian cancer. Int. J. Mol. Sci. 19, 2512. 10.3390/ijms19092512. [PubMed: 30149579]

19. Liang ZQ, Gao L, Chen JH, Dai WB, Su YS, and Chen G. (2021). Downregulation of the coiled-coil domain containing 80 and its perspective mechanisms in ovarian carcinoma: a Comprehensive Study. Int. J. Genomics 2021, 3752871. 10.1155/2021/3752871.

20. Leone V, Ferraro A, Schepis F, Federico A, Sepe R, Arra C, Langella C, Palma G, De Lorenzo C, Troncone G, et al. (2015). The cl2/dro1/ccdc80 null mice develop thyroid and ovarian neoplasias. Cancer Lett. 357, 535–541. 10.1016/j.canlet.2014.12.010. [PubMed: 25497869]

21. Zondervan KT, Becker CM, and Missmer SA (2020). N. Engl. J. Med. 382, 1244–1256. 10.1056/NEJMra1810764. [PubMed: 32212520]

22. Efremova M, Vento-Tormo M, Teichmann SA, and Vento-Tormo R. (2020). CellPhoneDB: inferring cell-cell communication from combined expression of multi-subunit ligand-receptor complexes. Nat. Protoc. 15, 1484–1506. 10.1038/s41596-020-0292-x. [PubMed: 32103204]

23. Simpson KD, Templeton DJ, and Cross JV (2012). Macrophage migration inhibitory factor promotes tumor growth and metastasis by inducing myeloid-derived suppressor cells in the tumor microenvironment. J. Immunol. 189, 5533–5540. 10.4049/jimmunol.1201161. [PubMed: 23125418]

24. Basisty N, Kale A, Jeon OH, Kuehnemann C, Payne T, Rao C, Holtz A, Shah S, Sharma V, Ferrucci L, et al. (2020). A proteomic atlas of senescence-associated secretomes for aging biomarker development. PLoS Biol. 18, e3000599. 10.1371/journal.pbio.3000599.

25. Yu W, Uzun Y, Zhu Q, Chen C, and Tan K. (2020). scATAC-pro: a comprehensive workbench for single-cell chromatin accessibility sequencing data. Genome Biol. 21, 94. 10.1186/s13059-020-02008-0. [PubMed: 32312293]

26. Muto Y, Wilson PC, Ledru N, Wu H, Dimke H, Waikar SS, and Humphreys BD (2021). Single cell transcriptional and chromatin accessibility profiling redefine cellular heterogeneity in the adult human kidney. Nat. Commun. 12, 2190. 10.1038/s41467-021-22368-w. [PubMed: 33850129]

27. Pervolarakis N, Nguyen QH, Williams J, Gong Y, Gutierrez G, Sun P, Jhutty D, Zheng GXY, Nemec CM, Dai X, et al. (2020). Integrated single-cell transcriptomics and chromatin accessibility analysis reveals regulators of mammary epithelial cell identity. Cell Rep. 33, 108273. 10.1016/j.celrep.2020.108273.

28. Regner MJ, Wisniewska K, Garcia-Recio S, Thennavan A, Mendez-Giraldez R, Malladi VS, Hawkins G, Parker JS, Perou CM, Bae-Jump VL, and Franco HL (2021). A multi-omic single-cell landscape of human gynecologic malignancies. Mol. Cell 81, 4924–4941.e10. 10.1016/j.molcel.2021.10.013. [PubMed: 34739872]
29. Korsunsky I, Millard N, Fan J, Slowikowski K, Zhang F, Wei K, Baglaenko Y, Brenner M, Loh PR, and Raychaudhuri S. (2019). Fast, sensitive and accurate integration of single-cell data with Harmony. Nat. Methods 16, 1289–1296. 10.1038/s41592-019-0619-0. [PubMed: 31740819]
30. Lynch MD, and Watt FM (2018). Fibroblast heterogeneity: implications for human disease. J. Clin. Invest. 128, 26–35. 10.1172/JCI93555. [PubMed: 29293096]
31. Weirauch MT, Yang A, Albu M, Cote AG, Montenegro-Montero A, Drewe P, Najafabadi HS, Lambert SA, Mann I, Cook K, et al. (2014). Determination and inference of eukaryotic transcription factor sequence specificity. Cell 158, 1431–1443. 10.1016/j.cell.2014.08.009. [PubMed: 25215497]
32. Cheng ZY, He TT, Gao XM, Zhao Y, and Wang J. (2021). ZBTB transcription factors: key regulators of the development, differentiation and effector function of T cells. Front. Immunol. 12, 713294. 10.3389/fimmu.2021.713294.
33. Kleiman E, Jia H, Loguercio S, Su AI, and Feeney AJ (2016). YY1 plays an essential role at all stages of B-cell differentiation. Proc. Natl. Acad. Sci. USA 113, E3911–E3920. 10.1073/pnas.1606297113. [PubMed: 27335461]
34. Castaneda M, Hollander P.d., and Mani SA (2022). Forkhead box transcription factors: double-edged swords in cancer. Cancer Res. 82, 2057–2065. 10.1158/0008-5472. [PubMed: 35315926]
35. Haybar H, Shahrabi S, Rezaeeyan H, Shirzad R, and Saki N. (2019). Endothelial cells: from dysfunction mechanism to pharmacological effect in cardiovascular disease. Cardiovasc. Toxicol. 19, 13–22. 10.1007/s12012-018-9493-8. [PubMed: 30506414]
36. Lengyel E, Wang H, Stepp E, Juarez J, Wang Y, Doe W, Pfarr CM, and Boyd D. (1996). Requirement of an upstream AP-1 motif for the constitutive and phorbol ester-inducible expression of the urokinase-type plasminogen activator receptor gene. J. Biol. Chem. 271, 23176–23184. 10.1074/jbc.271.38.23176. [PubMed: 8798512]
37. Javellana M, Eckert MA, Heide J, Zawieracz K, Weigert M, Ashley S, Stock E, Chapel D, Huang L, Yamada SD, et al. (2022). Neoadjuvant chemotherapy induces genomic and transcriptomic changes in ovarian cancer. Cancer Res. 82, 169–176. 10.1158/0008-5472.CAN-21-1467. [PubMed: 34737212]
38. Yao Y, Yao J, and Boström KI (2019). SOX transcription factors in endothelial differentiation and endothelial-mesenchymal transitions. Front. Cardiovasc. Med. 6, 30. 10.3389/fcvm.2019.00030. [PubMed: 30984768]
39. Abbadie C, Pluquet O, and Pourtier A. (2017). Epithelial cell senescence: an adaptive response to pre-carcinogenic stresses? Cell. Mol. Life Sci. 74, 4471–4509. 10.1007/s00018-017-2587-9. [PubMed: 28707011]
40. Banz C, Ungethuem U, Kuban RJ, Diedrich K, Lengyel E, and Hornung D. (2010). The molecular signature of endometriosis-associated endometroid ovarian cancer differs significantly from endometriosis-independent endometroid ovarian cancer. Fertil. Steril. 94, 1212–1217. 10.1016/j.fertnstert.2009.06.039. [PubMed: 19643405]
41. Jin A, Chen H, Wang C, Tsang LL, Jiang X, Cai Z, Chan HC, and Zhou X. (2014). Elevated expression of CD147 in patients with endometriosis and its role in regulating apoptosis and migration of human endometrial cells. Fertil. Steril. 101, 1681–1687.e1. 10.1016/j.fertnstert.2014.02.007. [PubMed: 24661733]
42. Wang C, Jin A, Huang W, Tsang LL, Cai Z, Zhou X, Chen H, and Chan HC (2015). Up-regulation of Bcl-2 by CD147 through ERK activation results in abnormal cell survival in human endometriosis. J. Clin. Endocrinol. Metab. 100, E955–E963. 10.1210/jc.2015-1431. [PubMed: 25996258]
43. Zheng M, Long J, Chelariu-Raicu A, Mullikin H, Vilsmaier T, Vattai A, Heidegger HH, Batz F, Keckstein S, Jeschke U, et al. (2021). Identification of a novel tumor microenvironment prognostic signature for advanced-stage serous ovarian cancer. Cancers 13, 3343. 10.3390/cancers13133343. [PubMed: 34283076]

44. Perets R, and Drapkin R. (2016). It's totally tubular Riding the new wave of ovarian cancer research. Cancer Res. 76, 10–17. 10.1158/0008-5472.CAN-15-1382. [PubMed: 26669862]
45. Wang S, Zheng Y, Li J, Yu Y, Zhang W, Song M, Liu Z, Min Z, Hu H, Jing Y, et al. (2020). Single-cell transcriptomic atlas of primate ovarian aging. Cell 180, 585–600.e19. 10.1016/j.cell.2020.01.009. [PubMed: 32004457]
46. Akhmedkhanov A, Zeleniuch-Jacquotte A, and Toniolo P. (2001). Role of exogenous and endogenous hormones in endometrial cancer: Review of the evidence and research perspectives. Ann. N. Y. Acad. Sci. 943, 296–315. 10.1111/j.1749-6632.2001.tb03811.x. [PubMed: 11594550]
47. Fornes O, Castro-Mondragon JA, Khan A, van der Lee R, Zhang X, Richmond PA, Modi BP, Correard S, Gheorghe M, Baranavsic', D., et al. (2020). JASPAR 2020: update of the open-access database of transcription factor binding profiles. Nucleic Acids Res. 48, D87–D92. 10.1093/nar/gkz1001. [PubMed: 31701148]
48. DePasquale EAK, Schnell DJ, Van Camp PJ, Valiente-Aland´ı Í, Blaxall BC, Grimes HL, Singh H, and Salomonis N. (2019). DoubletDecon: deconvoluting doublets from single-cell RNA-sequencing data. Cell Rep. 29, 1718–1727.e8. 10.1016/j.celrep.2019.09.082. [PubMed: 31693907]
49. Stuart T, Butler A, Hoffman P, Hafemeister C, Papalexi E, Mauck WM 3rd, Hao Y, Stoeckius M, Smibert P, and Satija R. (2019). Comprehensive integration of single-cell data. Cell 177, 1888–1902.e21. 10.1016/j.cell.2019.05.031. [PubMed: 31178118]
50. Hao Y, Hao S, Andersen-Nissen E, Mauck WM 3rd, Zheng S, Butler A, Lee MJ, Wilk AJ, Darby C, Zager M, et al. (2021). Integrated analysis of multimodal single-cell data. Cell 184, 3573–3587.e29. 10.1016/j.cell.2021.04.048. [PubMed: 34062119]
51. Schep AN, Wu B, Buenrostro JD, and Greenleaf WJ (2017). ChromVAR: inferring transcription-factor-associated accessibility from single-cell epigenomic data. Nat. Methods 14, 975–978. 10.1038/nmeth.4401. [PubMed: 28825706]
52. Ko SY, Ladanyi A, Lengyel E, and Naora H. (2014). Expression of the homeobox gene HOXA9 in ovarian cancer induces peritoneal macrophages to acquire an M2 tumor-promoting phenotype. Am. J. Pathol. 184, 271–281. 10.1016/j.ajpath.2013.09.017. [PubMed: 24332016]
53. Javellana M, Eckert M, and Lengyel E. (2019). Human Fallopian Tube and Ovary Dissociation for Single Cell RNA-Seq. 10.17504/protocols.io.bfudjns6.
54. Karst AM, and Drapkin R. (2012). Primary culture and immortalization of human fallopian tube secretory epithelial cells. Nat. Protoc. 7, 1755–1764. 10.1038/nprot.2012.097. [PubMed: 22936217]
55. Macosko EZ, Basu A, Satija R, Nemesh J, Shekhar K, Goldman M, Tirosh I, Bialas AR, Kamitaki N, Martersteck EM, et al. (2015). Highly parallel genome-wide expression profiling of individual cells using nanoliter droplets. Cell 161, 1202–1214. 10.1016/j.cell.2015.05.002. [PubMed: 26000488]
56. Zheng GXY, Terry JM, Belgrader P, Ryvkin P, Bent ZW, Wilson R, Ziraldo SB, Wheeler TD, McDermott GP, Zhu J, et al. (2017). Massively parallel digital transcriptional profiling of single cells. Nat. Commun. 8, 14049. 10.1038/ncomms14049. [PubMed: 28091601]
57. Hafemeister C, and Satija R. (2019). Normalization and variance stabilization of single-cell RNA-seq data using regularized negative binomial regression. Genome Biol. 20, 296. 10.1186/s13059-019-1874-1. [PubMed: 31870423]
58. Butler A, Hoffman P, Smibert P, Papalexi E, and Satija R. (2018). Integrating single-cell transcriptomic data across different conditions, technologies, and species. Nat. Biotechnol. 36, 411–420. 10.1038/nbt.4096. [PubMed: 29608179]

Highlights

- A single-cell atlas of the normal postmenopausal ovary and fallopian tube is shown
- Isthmus, ampulla, and fimbria share cell types but differ in chromatin accessibility
- Fallopian tube epithelial cells express genes associated with ovarian cancer risk
- Postmenopausal ovaries contain stromal cells expressing aging/senescence genes

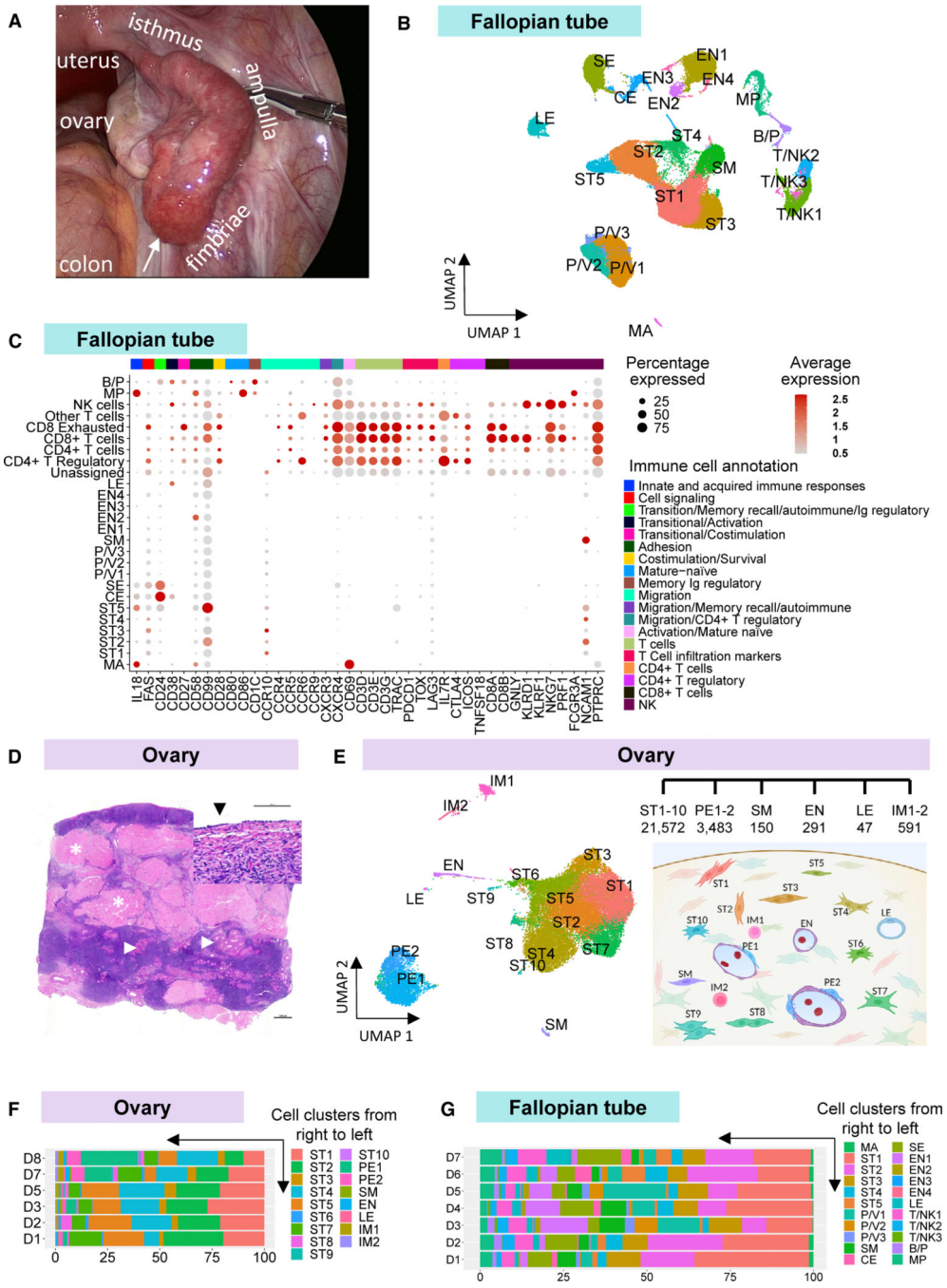

Figure 1. Single-cell RNA sequencing (scRNA-seq) reveals cell types of the normal human postmenopausal FTs and ovaries

(A) Intraoperative image of the right ovary, right side of the uterine fundus, I (the FT segment closest to the uterus), A, and the distal end of the FT (F). The fimbrial end extends over the ovary, allowing direct contact between the epithelium of the F (arrow) and the ovarian surface.

(B) Cell types found in the normal postmenopausal FT. A UMAP plot shows the 22 cell clusters identified in the FT using scRNA-seq. Data include F (n = 6), A (n = 6), and I (n = 6) for seven donors. Cell types are abbreviated as follows: ST1–ST5, 5 clusters of stromal

cells; T/NK1–T/NK3, 3 clusters of T and natural killer cells; SE, secretory epithelial; LE, lymphatic endothelial; SM, smooth muscle; MP, macrophage; P/V1–P/V3, 3 clusters of pericytes and vascular SM cells; CE, ciliated epithelial; EN1–EN4, 4 clusters of endothelial cells; B/P, B and plasma cells; MA, mast.

(C) Dot plot showing common gene expression markers found in IM and non-IM cell subtypes in the FT as identified by HIPPO analysis.

(D) Representative cross-section of a postmenopausal ovary (scale bar, 1,000 μm). In the medullary stroma, multiple arteries (arrowheads) and unresorbed corpora albicantia (asterisks) can be seen. Corpora albicantia show signs of multiple lifetime ovulation events that present as lobulated, eosinophilic structures composed of dense collagen fibers with occasional admixed fibroblasts. Inset: atrophic cortex at high magnification (scale bar, 100 μm). In the cellular stroma, no follicles are present, and only a few ovarian surface epithelial cells remain after surgical manipulation (black arrow).

(E) Right panel: cell types found in the normal postmenopausal ovary (n = 6). A UMAP plot shows the 17 cell clusters identified in the ovary using scRNA-seq. Cell types are abbreviated as follows: ST1–ST10, 10 clusters of ST cells; IM1/2, 2 clusters of immune cells; PE1/2, perivascular EN cells. Left panel: graphic depiction of cell subclusters and number of cells identified in each subcluster in the ovary using scRNA-seq.

(F and G) Relative abundance of the 17 cell clusters identified in the postmenopausal ovary (F) and of the 22 cell clusters found in the postmenopausal FT (G) using scRNA-seq. The graphs show the individual percentage of each cell type by the individual donor.

See also Figure S1 and Tables S1, S2, S3, S4, and S5.

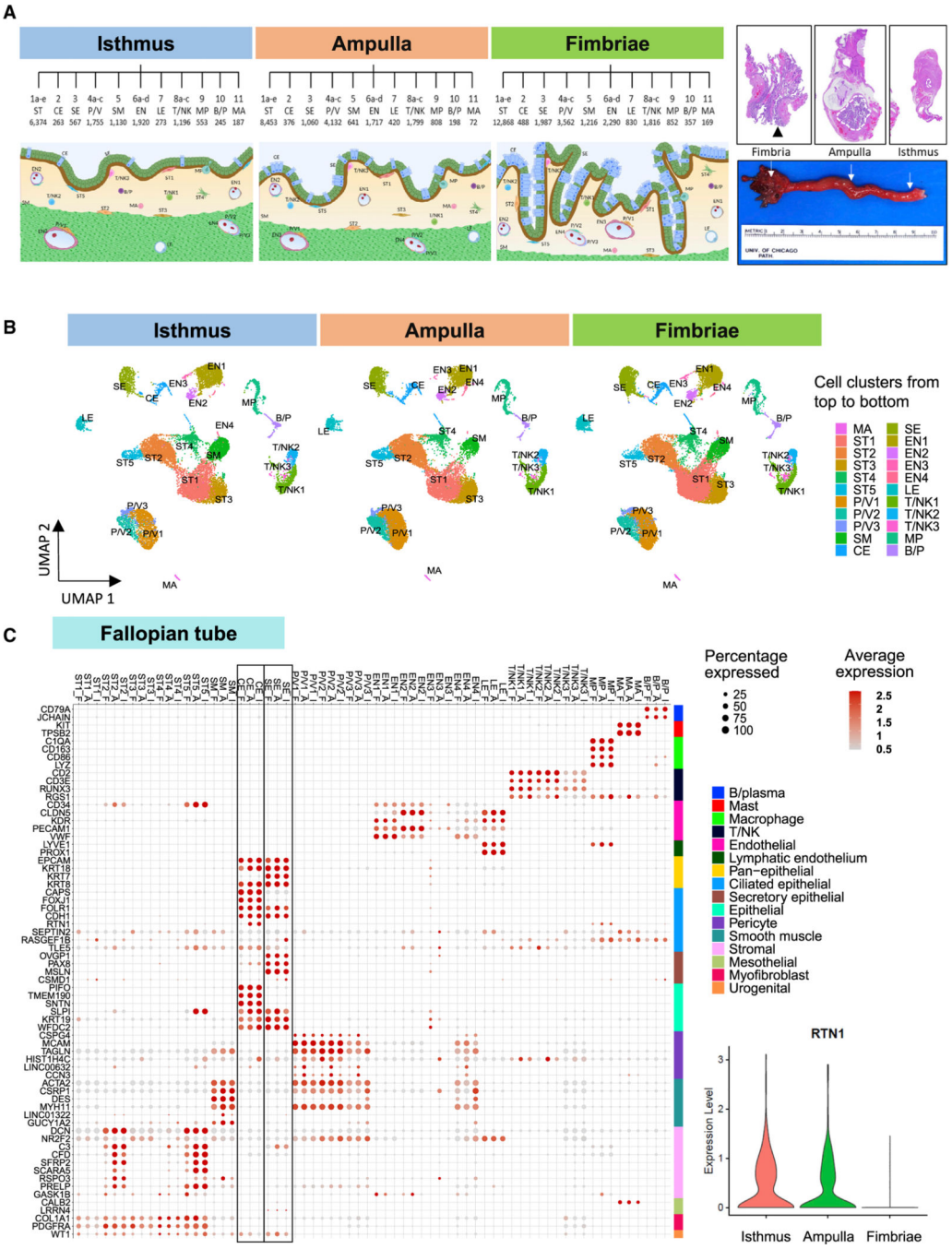

Figure 2. Gene expression in the I, A, and F regions of the postmenopausal FT

(A) Left panel: graphic depiction of cell subclusters and number of cells identified in each subcluster by anatomic region (I, A, and F) using scRNA-seq. Right panel: gross anatomic image of a normal FT, indicating the anatomic regions sampled and their corresponding cross-section H&E staining (1:40). Dashed lines around the FT lumen indicate the epithelium.

(B) UMAP of the 22 cellular clusters identified by scRNA-seq, divided by anatomic regions in the FT.

(C) Dot plot showing normalized expression levels of marker genes in common cell types identified in the I (n = 6), A (n = 6), and F (n = 6). SE and CE cells are framed. Also shown is a violin plot for Reticulon 1 (RTN1).
See also Figure S2.

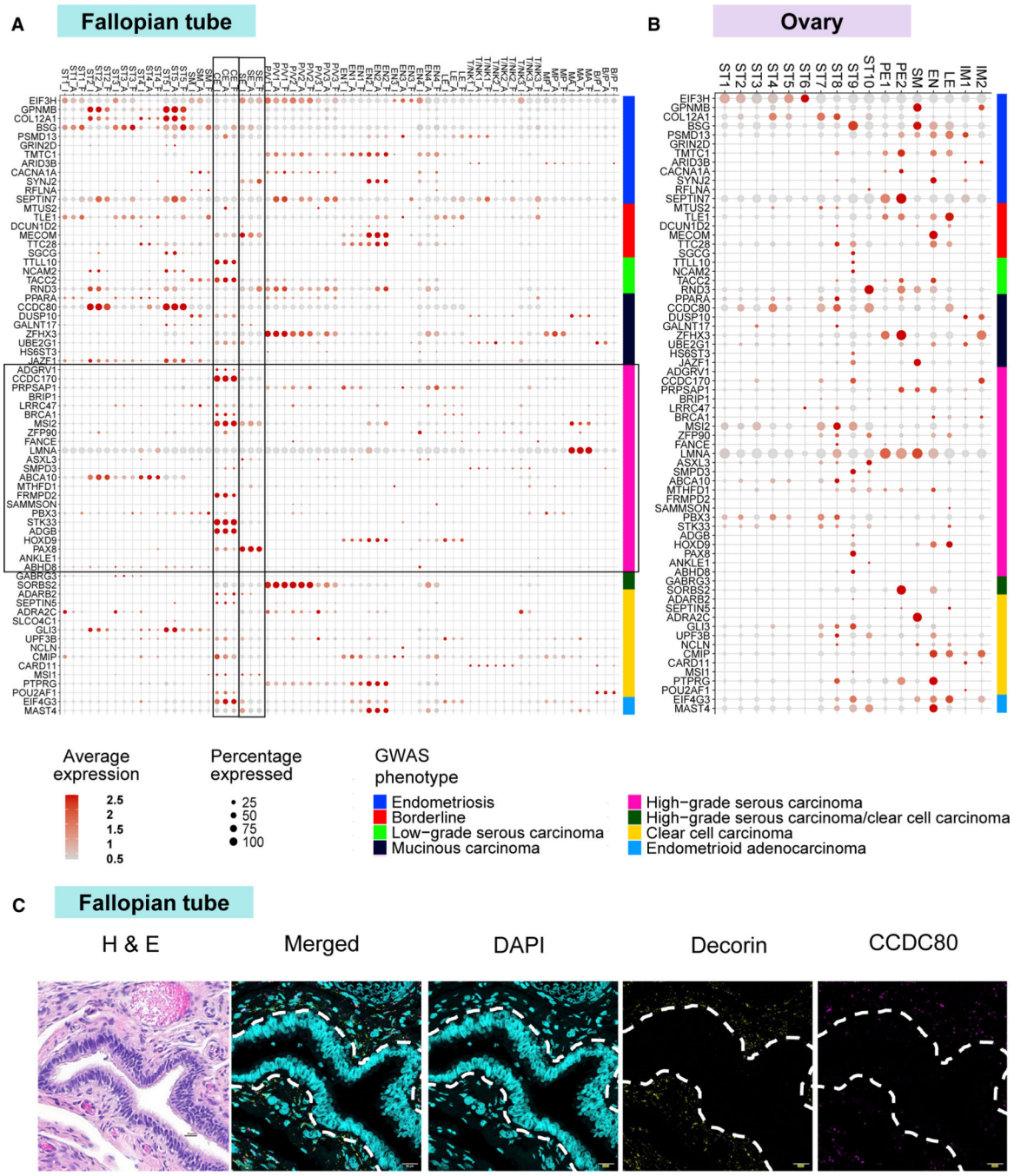

Figure 3. scRNA expression of genes identified in genome-wide association studies (GWASs) in different regions of the postmenopausal FT and ovary

(A and B) Dot plot showing cell type-specific expression of disease-specific genes as curated by GWASs in the FT (A) by anatomic region (I, A, F) and ovary (B).

(C) H&E and RNA fluorescence *in situ* hybridization (FISH) of decorin (DCN) and CCDC80 in the FT F. Every dot corresponds to one RNA transcript. Nuclei are stained with DAPI (cyan). Transcripts for DCN are shown in yellow and CCDC80 in magenta. Dashed white lines separate the epithelium from stroma in the FT (scale bars, 20 μm).

See also Figure S3 and Tables S7 and S8.

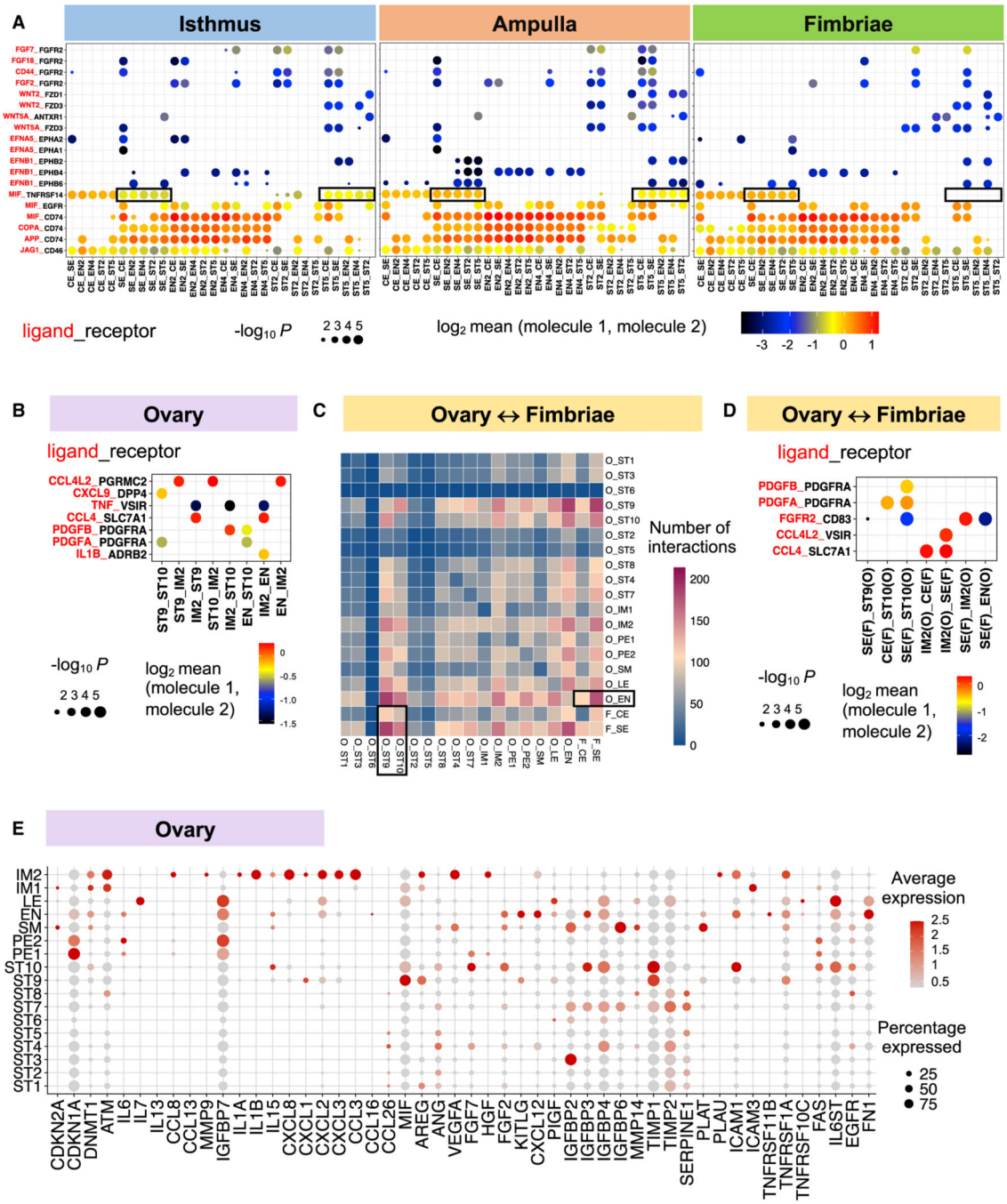

Figure 4. Ligand-receptor interactions and senescence-related gene expression in the FT and ovary

(A and B) Ligand-receptor interactions between different cell populations in the postmenopausal FT by anatomic region (A) and ovary (B) as detected by CellPhoneDB. y axis, ligands (red) and receptors (black); x axis, cell types with ligand-receptor interactions separated by underline. Black boxes indicate examples of significant changes between anatomic regions.

(C) Ovary-F interactions. A heatmap shows the number of interactions detected by CellPhoneDB among different cell types in the ovary and with SE and CE cells in the F of the FT.

(D) Ligand-receptor interactions between F and ovary, as detected by CellPhoneDB.

(E) Aging and senescence-related gene expression in the ovary. O, ovary.

See also Figure S4 and Tables S7 and S9.

Figure 5. Single-cell assay of transposase-accessible chromatin sequencing (scATAC-seq). Annotation of cell-types by label transfer from scRNA-seq in the postmenopausal FT and O.

(A and B) UMAP plot profiling of 41,515 cells (n = 4: I, A, F) identifying 18 cell clusters in the FT (A) and18,315 cells (n = 3) identifying 13 cell clusters in the O (B) using scATAC-seq. The labels before "–" are transferred from scRNA-seq data, and scATAC-seq-specific cluster labels are added as subgroup numbers after "–" (for example, there are now SE cell clusters −1 and −2).

(C and D) Relative abundance of the 18 cell clusters in the postmenopausal FT (C) and 13 cell clusters found in the O (D) using scATAC-seq after integrated analysis (label transfer from scRNA-seq). The graph shows the individual percentage of each cell type by the donor. (E and F) Heatmaps based on scATAC-seq data. Shown is TF activity by cell type in the FT including all 869 motifs available in the cisBP database (E) and specific TFs in the O (F). See also Figure S5 and Tables S5, S6, S10, and S11.

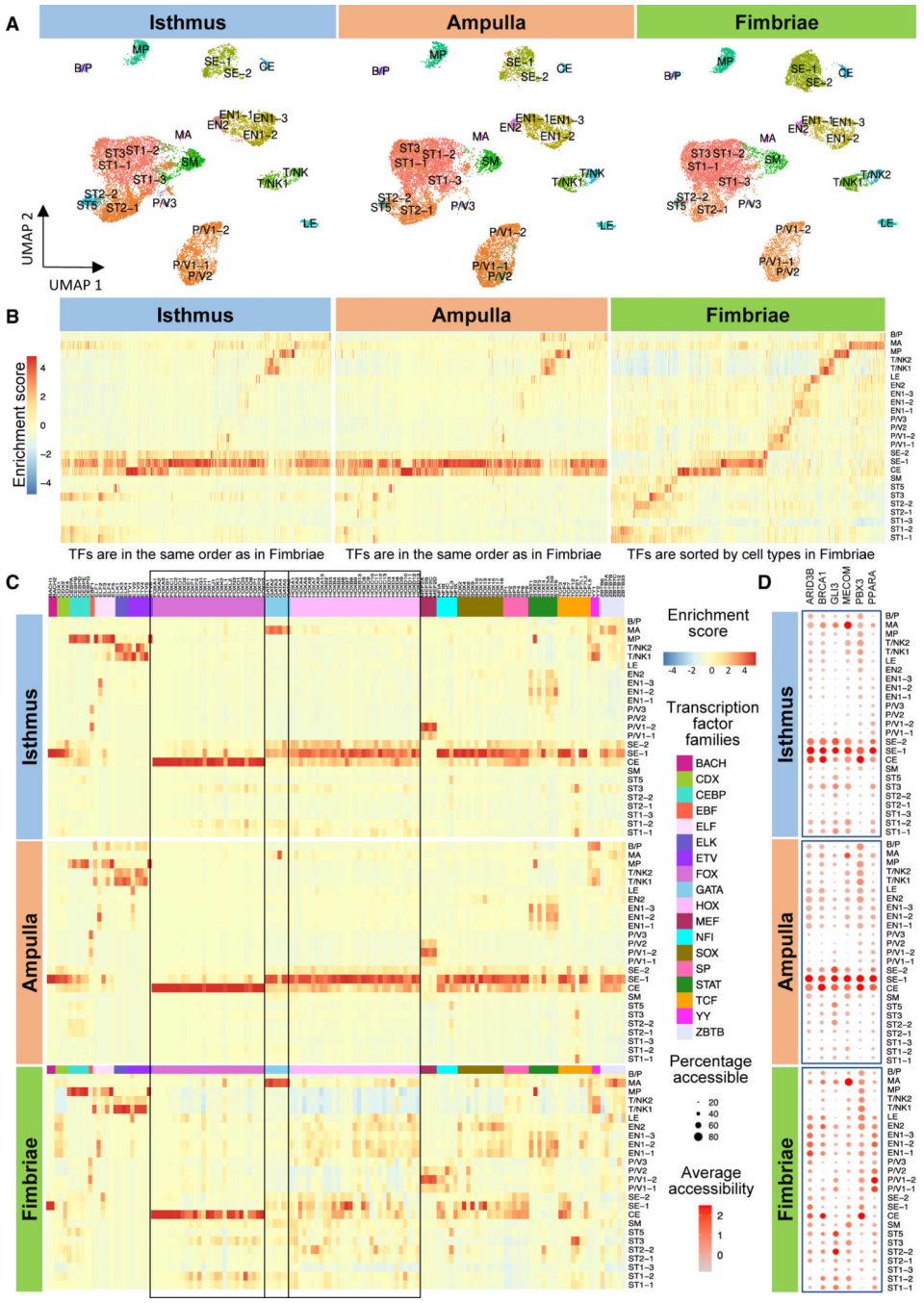

Figure 6. Clustering, cell type annotation, and transcription factor (TF) analysis of scATAC-seq in the different anatomic regions of the postmenopausal FT

(A) UMAP plot showing the 18 cell clusters identified in the I (n = 4), A (n = 3), and F (n = 4) by scATAC-seq after label transfer from scRNA-seq.

(B) Heatmap showing TF activity in the I, A, and F of the FT by cell type. Enrichment results were obtained from the cisBP database and contain 869 TF motifs. The order of TFs is the same across anatomic sites.

(C) Heatmap showing selected TFs in the I, A, and F.

(D) Dot plot showing chromatin accessibility of TFs of GWAS genes in Figure 3 by anatomic site and cell type.
See also Figure S6 and Table S7.

KEY RESOURCES TABLE

REAGENT or RESOURCE	SOURCE	IDENTIFIER
Antibodies		
Anti-mouse FOXJ1 Clone 2A5	eBioscience	Cat#14–9965-82; RRID:AB_1548835
Anti-mouse CD68 Clone PG-M1	Agilent	Cat#M0876; RRID:AB_2074844
Anti-mouse CD45 Clone 2b11+ PD7/26	Agilent	Cat#M0701; RRID:AB_2314143
Anti-mouse Pan Cytokeratin Clone [AE1/AE3]	Biocare Medical	Cat#CM011; RRID:AB_2811020
Anti-mouse Vimentin Clone V9	Agilent	Cat#M0725; RRID:AB_10013485
Anti-mouse PGR Clone 16	Leica Biosystems	Cat#NCL-PGR-312; RRID:AB_442125
Anti-mouse ER Clone 6F11	Leica Biosystems	Cat#PA0009; RRID:AB_2827388
Anti-rabbit PAX8	Proteintech	Cat#10336–1-AP; RRID:AB_2236705
Anti-rabbit EPCAM	Sigma-Aldrich	Cat#HPA026761; RRID:AB_1848198
Anti-mouse WT1 Clone 6F-H2	Thermo Fisher Scientific	Cat#MA1–46028; RRID:AB_962464
Anti-mouse CK7 Clone OV-TL12/30	Agilent	Cat#GA61961–2; RRID:AB_2925219
PAX8 Taqman probe Hs00247586_m1	Thermo Fisher Scientific	Cat#4448892
ESR1 Taqman probe Hs0146816_m1	Thermo Fisher Scientific	Cat#4331182
PGR Taqman probe Hs01556702_mq	Thermo Fisher Scientific	Cat#4331182
Vimentin Taqman probe Hs00958111_m1	Thermo Fisher Scientific	Cat#4453320
Barcode beads MACOSKO-2011–10 (V+)	Thermo Fisher Scientific	Cat#NC1513163
Exonuclease I from *E. coli*	New England BioLabs	Cat#M0293L
AMPure XP reagent	Beckman Coulter	Cat#A63880
Nextera XT DNA kit	Illumina	Cat#FC-131–1096
Biological samples		
Human fallopian tubes and ovaries	University of Chicago Medical Center	IRB 13–372B
Primary human fallopian tube epithelial cells	University of Chicago Medical Center	IRB 13–372B
Primary human fallopian tube stromal cells	University of Chicago Medical Center	IRB 13–372B
Primary human ovarian stromal cells	University of Chicago Medical Center	IRB 13–372B
Chemicals, peptides, and recombinant proteins		
Pronase from Streptomyces griseus	Sigma-Aldrich	Cat#10165921001

REAGENT or RESOURCE	SOURCE	IDENTIFIER
DNAse I recombinant from bovine pancreas	Millipore Sigma	Cat#4536282001
Collagenase IV from Clostridium histolyticum	Sigma-Aldrich	Cat#5138
Hyaluronidase from bovine testes	Sigma-Aldrich	Cat#H3884
EasySep RBC Depletion Reagent	Stemcell Tech	Cat#18170
Fetal Bovine Serum	Thermo Fisher Scientific	Cat#35–010-CV
DMEM with L-Glutamine	Corning	Cat#10–013-CV
Bovine serum albumin	Sigma Aldrich	Cat#A4503
Dulbeccos's phosphate-buffered saline	Gibco	Cat#21600–044
Trypan blue	Sigma-Aldrich	Cat#T8154
Annexin V	BD Biosciences	Cat#56547
Opti-MEM reduced serum media	Thermo Fisher Scientific	Cat#31985–070
Hanks balanced salt solution	Corning	Cat#21–022-CV
Critical commercial assays		
RNAscope LS Multiplex Fluorescent Reagent Kit	Advanced Cell Diagnostics	Cat#322800
Probe-Hs-DCN	Advanced Cell Diagnostics	Cat#589528
Probe Hs-CCDC80-C3 target: 2600–3557 of NM_199511.3	Advanced Cell Diagnostic	Cat#1153168-C3
REAGENT or RESOURCE	SOURCE	IDENTIFIER
Chromium Next GEM Single Cell 3′ Reagent Kit v3, 16rxns	10x Genomics	Cat#1000075
Chromium Next GEM Single Cell ATAC Reagent Kits v1.1, 16rxns	10x Genomics	Cat#10000283
Agilent high sensitivity DNA kit	Agilent	Cat#5067–4626
iTaq universal probes supermix	Bio-Rad	Cat#1725134
Deposited data		
CellPhoneDB database v2.0.0.	Efremova, et al.[22]	https://www.cellphonedb.org/
cisBP	Weirauch, Yang et al.[31]	http://cisbp.ccbr.utoronto.ca
Dataset of normal epithelial cells	Hu, et al.[11]	https://www.ncbi.nlm.nih.gov/geo/query/acc.cgi?acc=GSE139079
Postmenopausal patient data	Dinh, et al.[7]	https://www.ncbi.nlm.nih.gov/geo/query/acc.cgi?acc=GSE151214
Human reference genome NCBI build 38, hg38	Genome Reference Consortium	https://www.ncbi.nlm.nih.gov/assembly/GCF_000001405.26/
JASPAR database	Fornes, Castro-Mondragon et al.[47]	https://jaspar.genereg.net

REAGENT or RESOURCE	SOURCE	IDENTIFIER
Processed scRNA- and scATAC-seq data	Cellxgene	https://cellxgene.cziscience.com/collections/d36ca85c-3e8b-444c-ba3e-a645040c6185
Raw scRNA- and scATAC-seq data	EGA	EGAS00001006780
Oligonucleotides		
Custom Read1 primer GCCTGTCCGCGGAAGCAGT GGTATCAACGCAGAGTAC	N/A	N/A
Software and algorithms		
GraphPad Prism	GraphPad	N/A
Fiji	NIH, Fiji developers	https://imagej.net/software/fiji/
NIS-Elements version:AR5.30.05 64 bit	Nikon	N/A
Bio-Rad CFX Maestro v2.2	Bio-Rad	N/A
Cell Ranger for gene expression	10x Genomics	https://support.10xgenomics.com/single-cell-gene-expression/software/overview/welcome
Cell Ranger ATAC 1.2	10x Genomics	https://support.10xgenomics.com/single-cell-atac/software/overview/welcome
DoubletDecon	DePasquale, Schnell et al.[48]	https://github.com/EDePasquale/DoubletDecon
Seurat v4.0	Stuart, Butler et al.[49]	https://satijalab.org/seurat/
HIPPO	Kim and Chen,[8]	https://github.com/ChenMengjie/lightHippo
Signac v1.4.0	Hao, Hao et al.[50]	https://cran.r-project.org/web/packages/Signac/index.html
Harmony	Korsunsky, Millard et al.[29]	https://github.com/immunogenomics/harmony
chromVAR v3.14	Schep, Wu et al.[51]	https://bioc.ism.ac.jp/packages/3.14/bioc/html/chromVAR.html
Other		
Nikon Eclipse Ti2 microscope	Nikon	N/A
Qubit 3.0 Fluorometer	Invitrogen	Cat#Q33216
Agilent BioAnalyzer 2100	Agilent	Cat#G2939BA
CFX Opus 96 Real-time PCR system	Bio-Rad	Cat#12011319